Biologically Inspired Dynamic Thresholds
for Spiking Neural Networks
(Supplementary Material)

Jianchuan Ding[1]   **Bo Dong**[2*]   **Felix Heide**[2]
Yufei Ding[3]   **Yunduo Zhou**[1]   **Baocai Yin**[1]   **Xin Yang**[1*]
[1]Dalian University of Technology, Department of Computer Science
[2]Princeton University, Department of Computer Science
[3]University of California-Santa Barbara, Department of Computer Science

Supplementary Note 1: Spiking Neural Networks

Spiking Neural Network (SNN)

Various models for spiking neurons mathematically describe the properties of a cell in the nervous system with varying degrees of detail. Normally, three conditions are considered by these models: resting, depolarization, and hyperpolarization. When a neuron is resting, it maintains a constant membrane potential. The change in membrane potential can be either a decrease or an increase relative to the resting potential. An increase in the membrane potential is called depolarization, which enhances a cell's ability to generate an action potential; it is excitatory. In contrast, hyperpolarization describes a reduction in the membrane potential, which makes the associated cell less likely to generate an action potential, and, as such, is inhibitory. All inputs and outputs of a spiking neuron model are sequences of spikes.

A sequence of spikes is called a spike train and is defined as $s(t) = \Sigma_{t^{(f)} \in \mathcal{F}} \delta(t - t^{(f)})$, where $\mathcal{F}$ represents the set of times at which the individual spikes occur [1]. Typical spiking neuron models set the resting potential to 0. However, existing models achieve depolarization and hyperpolarization in substantially different ways. In the following, we review two commonly used models: the spike response model (SRM) [2] and leaky integrate-and-fire (LIF) model [3].

Spike Response Model (SRM) An SRM first converts an incoming spike train $s_i(t)$ into a spike response signal as $(\varepsilon * s_i)(t)$, where $\varepsilon(\cdot)$ is a spike response kernel. Then, the generated spike response signal is scaled by a synaptic weight w_i. Depolarization is achieved by summing all the scaled spike response signals: $\Sigma_i w_i(\varepsilon * s_i)(t)$. When incoming spike trains trigger a spike $s(t)$, the SRM models hyperpolarization by defining a refractory potential as $(\zeta * s)(t)$, where $\zeta(\cdot)$ is a refractory kernel. With an SRM, a feedforward SNN architecture with n_l layers can be defined. Given N^l incoming spike trains at layer l, $s_i^l(t)$, the forward propagation process of the network is mathematically defined as follows [2, 1]:

$$v_i^{l+1}(t) = \sum_{j=1}^{N^l} w_{ij}(\varepsilon * s_j^l)(t) + (\zeta * s_i^{l+1})(t-1), \tag{1}$$

$$s_i^{l+1}(t) = f_s(v_i^{l+1}(t)), \tag{2}$$

$$f_s(v) : v \to s, s(t) := s(t) + \delta(t - t^{(f+1)}), \tag{3}$$

$$t^{f+1} = \min\{t : v(t) = \Theta, t > t^{(f)}\}, \tag{4}$$

---

*Corresponding author xinyang@dlut.edu.cn; bo.dong@princeton.edu

36th Conference on Neural Information Processing Systems (NeurIPS 2022).

where $f_s(\cdot)$ is a spike function and Θ is the membrane potential threshold, which is static and the same for all neurons in the network. This static threshold is the one that we replace with the proposed dynamic threshold.

Leaky Integrate-and-Fire (LIF) An LIF model is a simplified variant of an SRM. This scheme directly processes incoming spike trains and ignores the spike response kernel. Hyperpolarization is achieved by a simple decay function $f_d(\cdot)$. The forward propagation process of the network can be defined as:

$$v_i^{l+1}(t) = \sum_{j=1}^{N^l} w_{ij} s_j^l(t) + v_i^{l+1}(t-1) f_d(s_i^{l+1}(t-1)) + b_i^{l+1}, \tag{5}$$

$$s_i^{l+1}(t) = f_s(v_i^{l+1}(t)), \tag{6}$$

$$f_d(s(t)) = \begin{cases} D & s(t) = 0 \\ 0 & s(t) = 1, \end{cases} \tag{7}$$

where b_i^{l+1} is an adjustable bias that is learned to mimic a dynamic threshold behavior. However, the biases of this model are static during forwarding propagation. In contrast, the proposed dynamic threshold is dynamic and automatically adapts to membrane potentials.

Supplementary Note 2: Related Mathematical Definitions

In this section, we provide mathematical definitions for DT1, DT2, and Loihi weight transferring. In addition, we formally define the proposed homeostasis metrics.

DT1 Hao [4] noted that neurons do not (or barely) fire when their thresholds are too large, which can negatively affect model performance. Therefore, they proposed DT1 to slow threshold growth. For the i-th neuron in the l-th layer, DT1 at timestamp t is mathematically defined as:

$$\Theta_{DT1,i}^l(t) = \Theta_{const} + (-\Theta_{DT1,i}^l(t-1) + \frac{\Theta_{initial}}{|2\Theta_{DT1,i}^l(t-1) - \Theta_{initial}|} \sum_{i=1}^{n^l} s_i^l(t)), \tag{8}$$

where Θ_{const} and $\Theta_{initial}$ are two hyperparameters; the dynamic threshold is mainly controlled by a dynamic scaling factor $\frac{\Theta_{initial}}{|2\Theta_{DT1,i}^l(t-1) - \Theta_{initial}|}$; n^l is the total number of neurons in the l-th layer. For fair comparisons with other competing approaches, we apply grid search to find the optimal values of $\Theta_{initial}$ and Θ_{const} and ensure that the host SNNs of DT1 offer similar success rates (SRs) in the static obstacle avoidance task to those of other approaches. Based on the grid search, $\Theta_{initial}$ is set to 10.0; 0.5 and 0.2 are the optimal values of Θ_{const} for the LIF-based and SRM-based host SNNs, respectively.

DT2 Inspired by the observed homeostasis in biology, Kim [5] proposed DT2 to maintain neurons' firing rates at a predefined constant target frequency. Mathematically, for the i-th neuron in the l-th layer, DT2 at timestamp t is defined as:

$$\Theta_{DT2,i}^l(t) = \Theta_{DT2,i}^l(t-1) + (\sum_{i=1}^{n^l} s_i^l(t)) - f_{target}^l) \times \Theta_{DT2,i}^l(t-1) \times \gamma, \tag{9}$$

where f_{target}^l is the predefined constant target frequency; γ is a homeostasis factor that determines the threshold changing rate. Based on our grid search, we set f_{target}^l to 85 (1/3 of 256) for the three 256-neuron layers and γ to 0.004 to achieve the same static obstacle avoidance performance as that of other competing SNNs.

8-Bit Loihi Weights In our weight uncertainty (WU) experiments, we scale and round up the learned floating-point synaptic weights to low-precision 8-bit weights. The weight scaling process is defined as:

2

$$r^l = \frac{w_{\text{max}}^{\text{Loihi}}}{w_{\text{max}}^l}, \tag{10}$$

$$w_{ij}^{(l)(\text{Loihi})} = \text{round}(r^l w_{ij}^l), \tag{11}$$

$$\Theta_i^{(l)(\text{Loihi})}(t) = \text{round}(r^l \Theta_i^l(t)), \tag{12}$$

$$v_i^l(t) = v_i^{(l)(\text{Loihi})}(t)/r^l, \tag{13}$$

where r^l is the rescaling ratio of layer l; w_{max}^{Loihi} is the maximum weight that Loihi supports; w_{max}^l is the maximum weight of the l-th layer of the host SNN; w_{ij}^l is the synaptic weight between the i-th neuron in the l-th layer and the j-th neuron in the $(l-1)$-th layer, and $w_{ij}^{(l)(\text{Loihi})}$ is the corresponding rescaled weight on Loihi; $\Theta_i^l(t)$ and $\Theta_i^{(l)(\text{Loihi})}(t)$ are the original membrane threshold and the corresponding threshold for Loihi of the i-th neuron in the l-th layer at timestamp t, respectively; round(x) is a rounding function that returns the rounded version of x. Notably, to estimate $\Theta_i^l(t)$, we need to know the original membrane potentials. However, all the membrane potentials on Loihi are rescaled. Therefore, to obtain the original membrane potentials, we need to reverse the process defined in Eq 13.

Homeostasis Metrics We leverage three statistical metrics to quantify the homeostasis of an SNN. Mathematically, they are defined as follows:

$$\text{FR}_m = \mu(\text{FR}_m^p) \quad \text{for} \quad p = 1, 2, ..., P, \tag{14}$$

$$\text{FR}_{std}^m = \mu(\text{FR}_{std}^p) \quad \text{for} \quad p = 1, 2, ..., P, \tag{15}$$

$$\text{FR}_{std}^s = \sigma(\text{FR}_{std}^p) \quad \text{for} \quad p = 1, 2, ..., P, \tag{16}$$

$$\text{FR}_m^p = \mu(f_i^{l,p}) \quad \text{for } i = 1, 2, ..., N^l \quad l = 1, 2, ..., L, \tag{17}$$

$$\text{FR}_{std}^p = \sigma(f_i^{l,p}) \quad \text{for } i = 1, 2, ..., N^l \quad l = 1, 2, ..., L, \tag{18}$$

$$f_i^{l,p} = \frac{\sum_{t^p=1}^{T^p} s_i^l(t^p)}{T^p}, \tag{19}$$

where, T^p is the time taken for the p-th trial and $f_i^{l,p}$ is the firing rate of the i-th neuron in the l-th layer during the p-th trial. FR_m^p denotes the mean firing rate of all neurons of an SNN during the p-th trial, and FR_{std}^p is the standard deviation of all neuron firing rates for an SNN during the p-th trial. The definitions of FR_m, FR_{std}^m, and FR_{std}^s are defined in the main paper.

3
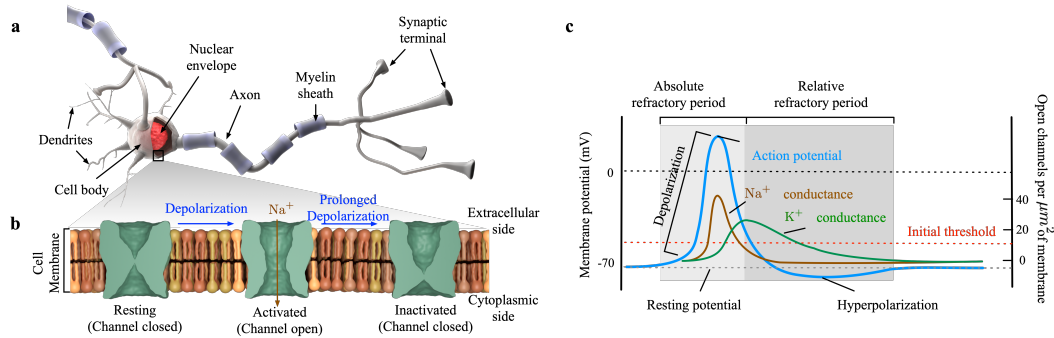
Figure 1: a. The structure of a neuron. b. We demonstrate a sodium (Na^+) voltage-gated channel under resting, activated, and inactivated (refractory) states. The Na^+ channel enters an inactivated state after depolarization and returns to a resting state only after the membrane potential is restored to its resting potential. c. The process of action potential generation, which is based on the Hodgkin-Huxley model [6], involves the sequential opening of voltage-gated Na^+ and K^+ channels. The Na^+ and K^+ conductance curves are adapted from the Hodgkin-Kuxley model [6].

Supplementary Note 3: Biological Concepts

A typical biological neuron has four morphological regions: a cell body, dendrites, an axon, and synaptic terminals. Inside the cell body (the soma), a nuclear envelope contains the cell's genes. The short tree-like dendrites branch out from the cell body, and they are the main apparatus for receiving incoming signals from other neurons. The long tubular axon covered by the myelin sheath extends some distance from the cell body and carries action potential to other neurons through synaptic terminals. A typical nerve neuron is illustrated in Figure 1a.

In a nerve cell that is at rest, the extracellular surface of the cell membrane has an excess positive charge, while the cytoplasmic side has an excess negative charge. The cell membrane maintains the separation of charge as a barrier against the diffusion of ions; see Figure 1b. The electrical potential difference across the membrane is defined as the membrane potential, which has three different statuses: resting, depolarization, and hyperpolarization. At rest, no net charge movement across the membrane occurs, and the resting membrane potential is maintained. By convention, the potential outside the cell is defined as zero, and hence, the resting potential is a negative value. A net flow of cations or anions into or out of a cell disturbs the resting membrane, causing depolarization or hyperpolarization, respectively. Depolarization indicates less negative membrane potential, while hyperpolarization signifies more negative potential; see Figure 1c.

Dynamic Thresholds in Biological Neurons

The Hodgkin-Huxley model [6] has served as an archetype for compartmental models of the electrophysiology of biological membranes (see Figure 1a). Many numerical methods leverage the Hodgkin-Huxley model as their testbeds, which can be applied to more complex models [7, 8, 9]. We use the Hodgkin-Huxley model to introduce the concept of threshold in biological neurons. Based on the Hodgkin-Huxley model, an action potential is produced when the membrane potential is higher than a particular threshold; this involves the following sequence of processes. First, when the membrane potential is higher than a threshold, the associated depolarization opens sodium (Na^+) channels, resulting in an inward Na^+ current. By discharging the membrane capacitance, the inward current causes further depolarization and the opening of more Na^+ channels, resulting in a further increase in the inward current. Second, under prolonged depolarization, the voltage-gated Na^+ channels become inactive. Furthermore, after some delay, the voltage-gated potassium (K^+) channels begin to open, causing an outward K^+ current that tends to repolarize the membrane (see Figure 1b). The second process underlies the absolute refractory period [10], a period during which no action potential can be elicited. After that, with some K^+ channels being closed and some Na^+ channels

4

recovering from inactivation, the membrane enters a relative refractory period [10] (see Figure 1c). During this period, it is possible to trigger an action potential, but this requires a higher threshold.

Note that a small subthreshold depolarization cannot trigger an action potential, as it not only increases the inward Na^+ current but also increases the outward K^+ current [6]. Only at a specific membrane potential value does the net ionic current become inward, depositing a net positive charge on the inside of the membrane capacitance. This specific value is the potential (or spike) threshold [11].

The threshold changes dynamically, widely observed in the different nervous systems [12, 13, 14, 7, 15, 16, 17, 18, 19]. A thread of studies leverage the Hodgkin-Huxley model to verify the observed threshold dynamics [20, 7]. However, not all spike initiation dynamics of biological neurons can be accurately described by the Hodgkin-Huxley model [21].

5

Supplementary Note 4: Additional Details on Obstacle Avoidance Experiments

Experimental Setup

In the obstacle avoidance experiments, our evaluation baseline model and test environment are modified variants of the spiking actor network (SAN) [22] and its original simulated test environment, respectively. The SAN is a part of the spiking deep deterministic policy gradient (SDDPG) framework [22], which is a fully connected four-layer SNN (three 256-neuron hidden layers and one two-neuron output layer). This network maps a state s of a robot to a control action a. Specifically, a state $s = \{G_{dis}, G_{dir}, \nu, \omega, L\}$ is encoded into 24 Poisson spike trains as inputs of the SAN, and each spike train has T timesteps. G_{dis} and G_{dir} are the relative 1-D distances from the robot to the goal and a 2-D direction (right and left directions), respectively; ν and ω are the robot's 1-D linear and 2-D angular velocities (rightward and leftward angular velocities); L denotes the distance measurements obtained from a Robo Peak light detection and ranging (RPLIDAR) laser range scanner (range: 0.2-40 m), which has a field of view of 180 degrees with 18 range measurements, each with a 10-degree resolution. The two output spike trains are decoded to control the robot via an action $a = \{\nu_L, \nu_R\}$, where ν_L and ν_R are the left and right wheel speeds of the differential-drive mobile robot, respectively [22].
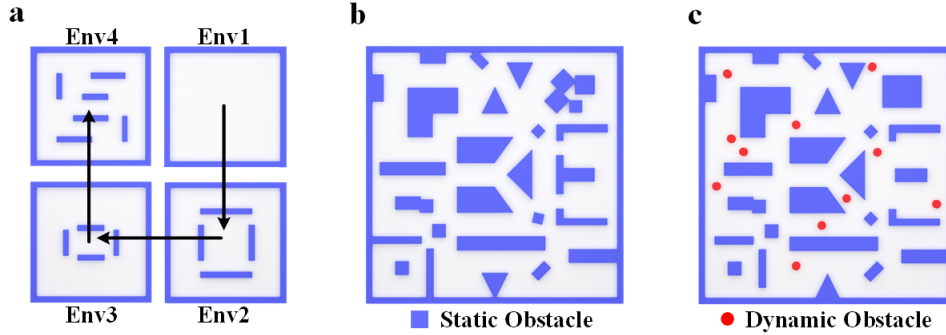
Figure 2: Illustrations of the training, static testing and dynamic testing environments. a. The training environments of the obstacle avoidance tasks. The training processes of all competing SNNs start from Env1 and end with Env4. b. Static testing environment. c. Dynamic testing environment. In addition to static obstacles, 11 dynamic obstacles are inserted.

Training

The SAN and its modified versions are trained with the original SDDPG framework. The training environments consist of four different maps, as shown in Figure 2a. In particular, during the training process, we set 100, 200, 300, and 400 start-goal pairs in the Env1, Env2, Env3, and Env4, respectively. The training starts from Env1 and ends with Env4. Following the training protocol described by Tang [22], the hyperparameters related to training are set as follows: $D = 0.75$ for the LIF; $\eta = 0.01$ and $\psi = 4.0$ for the dynamic energy threshold (DET); $C = 3.0$ for the dynamic temporal threshold (DTT); $\tau_s = \tau_r = 1.0$ for the SRM; collision reward $= -20$; goal reward $= 30$; step reward $= 15$; goal l_2 distance threshold $= 0.5$ m; obstacle l_2 distance threshold $= 0.35$ m; ϵ ranges for Env1 to Env4 of $(0.9, 0.1)$, $(0.6, 0.1)$, $(0.6, 0.1)$, and $(0.6, 0.1)$, respectively; and corresponding ϵ-decays of 0.999 for the four environments. During the training procedure, we set the batch size to 256 and the learning rates to 0.00001 for both the actor and critic networks. We use PyTorch [23] to train and test all competing SNNs with an i7-7700 CPU and an NVIDIA GTX 1080Ti GPU. We direct the readers to the SAN algorithm [22] for details.

Assessment—Success Rate

We evaluate the obstacle avoidance capabilities of the proposed method by using SR as a metric. The SR is the percentage of successful passes out of 200 trials. A successful pass is a trial in which the robot can reach its destination without touching any static or dynamic obstacle within 1000 steps. In addition to the SR, we also report the overtime percentage (OTP), the percentage of overtime trials

6

out of the total trials (200 trials), where overtime is defined as a trial in which the robot cannot reach the goal within 1000 steps but does not touch any obstacle.

We use the Gazebo simulator to construct a 20×20 m^2 static test environment (see Figure 2b) and adopt the randomly sampled 200 start-goal location pairs used for testing the SAN [22]. For fairness, we apply grid searches on all tunable hyperparameters to ensure that the SRs of all competing approaches are relatively the same (within $\pm 2\%$) when testing in the static testing environment. The quantitative experimental results obtained by all competing dynamic threshold methods in the static obstacle avoidance tasks are shown in Table 1. Due to space limits, we only report the experimental results based on $T = 5$ in the main manuscript. Here, we offer the quantitative performance with both $T = 5$ and $T = 25$.

Based on Table 1, compared to the SRs obtained with $T = 5$, the SRs obtained under $T = 25$ only change slightly ($\pm 0.5\%$), indicating that all competing SNNs are not sensitive to the T value in static obstacle avoidance tasks. The observations related to the T value also hold in the dynamic obstacle experiments (see Table 2). However, we observe that the SRs decrease as the T value increases for most degraded input and weight uncertainty experiments.

Tables 2, 3, and 4 show the quantitative performance of all competing approaches in dynamic obstacle, degraded inputs, and weight uncertainty experiments, respectively. The SRs are also shown in Figures 4a and b. In terms of the OTPs, we witness high levels of overtime trials in the "0.2" section of the degraded inputs condition and the "GN weight" section of the weight uncertainty condition. As discussed in the main manuscript, with the "0.2" setup, the three disturbed lasers generate more spikes than they are supposed to, making the robot more cautious. Thus, the robot's speed slows, leading to more overtime trials. As expected, adding Gaussian noise to the learned weights reduces the effectiveness of the avoidance policy. However, our approach faces the most negligible impact, offering the best SRs under all experimental results. In the following, we provide a more detailed analysis for each degraded condition.

Dynamic Obstacles As discussed, we introduce 11 dynamically moving cylinders to the static testing environment; see Figure 2c. Table 2 shows the corresponding experimental results obtained under this condition. Our approach delivers the highest SRs with both the LIF and SRM neuron models. Notably, under both the $T = 5$ and $T = 25$ settings, the proposed approach outperforms the runners-up by significant margins (by at least 9% over the LIF model and 12% over the SRM). The results demonstrate that the proposed bioinspired dynamic threshold scheme provides substantial environmental adaptability to the host SNNs. Since all the synaptic weights and static thresholds of both the SAN and the SAN with no resting operation (SAN-NR) are learned from the environments with static obstacles only, we expect that they cannot adapt well to an environment with dynamic objects. Surprisingly, compared to the static threshold scheme, the two heuristic dynamic threshold schemes, DT1 and DT2, obtain lower SRs. The threshold dynamics provided by DT1 rely on two hyperparameters, the constant potential and initial potential. DT2 requires a target firing count to be set. These hyperparameters are justified during the training process but fixed during testing. We believe that these hyperparameters dramatically impact the adaptability of the tested heuristic dynamic threshold schemes. In contrast, the dynamics offered by the proposed bioinspired dynamic energy-temporal threshold (BDETT) scheme are dynamically based on layerwise statistical cues.

Degraded Inputs In this experiment, as discussed in our main manuscript, in addition to the presence of dynamic obstacles, we disturb the obtained range measurements in three different ways: a) "0.2": we set the 3rd, 9th, and 15th laser ranges to 0.2 m. In this case, the three modified measurements always report obstacles in their perception fields even when none are present; b) "6.0": the ranges of the same three lasers are set to 6.0 m, which is the average visible range in the test environment. This means that the three lasers cannot perceive any object; c) "GN": we add Gaussian noise ($clip(s_{input} + \mathcal{N}(0, 1.0), 0.2, 6.0)$, as suggested in a study regarding long short-term memory with a local map critic (LSTM-LMC) [24]) to each of the 18 range measurements. The experimental results obtained under these settings are shown in Table 3.

In all degraded input experiments, the SRs offered by our BDETT scheme still remain the highest and outperform the runners-up by at least 10%. This reflects that the proposed dynamic threshold scheme provides the host SNNs with strong adaptability to all designed degraded inputs, which is highly desired and appreciated in mobile robot applications. In the "0.2" setup, the three disturbed lasers generate more spikes than they are supposed to, making the robot more cautious. All host SNNs obtain lower SRs than those obtained under the dynamic obstacle settings. However, the

7
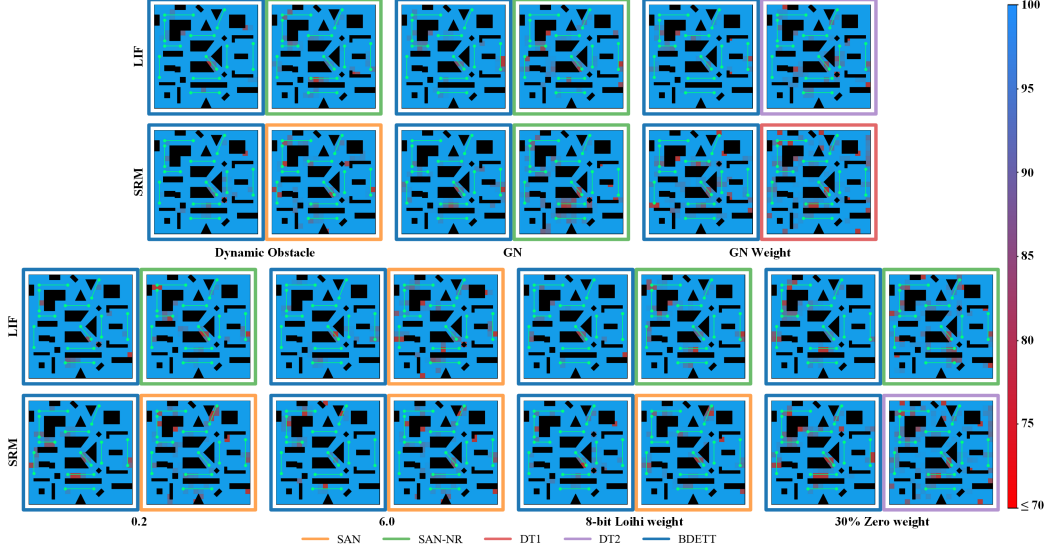
Figure 3: The success rate heatmaps. The heatmaps yielded by the best and runner-up performers under four different conditions indicate the areas with lower success rates (those shown in red).

SRM-based host SNNs are significantly impacted. We believe the reason for this is that the spike response and refractory kernels of the SRM amplify the intense spikes triggered by the three modified measurements. In the "6.0" experiments, the three modified measurements trigger fewer spikes, and the robot becomes more relaxed due to the 'hyperopia' effect. Therefore, we expect more failed passes than in the "0.2" setup. This is true for the LIF-based SNNs but not for the SRM-based SNNs. Since the three farsighted lasers reduce the signal amplification effects caused by the two kernels, the SRM-based SNNs perform better here than in the "0.2" experiments. Under the "GN" condition, the SRs of all competing host SNNs decrease, but our approach is the least affected and induces the lowest SR drops. Remarkably, under all degraded input experiments, the proposed BDETT improves upon the SRs of both the LIF-based and SRM-based baseline models (SAN-NR) by at least 10% and 17%, respectively. The success rates of the best and runner-up performers under "0.2" and "6.0" conditions are also qualitatively illustrated in Figure 3.

Weight Uncertainty Neuromorphic hardware (Loihi) achieves computing efficiency by sacrificing the weight precision, and an 8-bit integer normally yields the highest precision. Therefore, when deploying an SNN on neuromorphic hardware, one needs to scale and round up the learned floating-point synaptic weights to low-precision weights. We mimic this scenario by mapping the learned weights to Intel's Loihi 8-bit integer weights. The mapping equations are provided in Supplementary Note 2. In addition, we design two extra weight pollution experiments. "GN weight" involves adding Gaussian noise ($w_{ij} + \mathcal{N}(0, 0.05)$) to all synaptic weights; under "30% zero weight", we reandomly set 30% of the synaptic weights between every two adjacent layers to 0. To reduce the impact caused by the randomness introduced in the two additional experiments, we report the average SRs of 5-round tests.

As shown in Table 4, the proposed BDETT can effectively reduce the impact caused by degraded synaptic weights and deliver the best SRs under all experimental settings. Low-precision weight convergence slightly reduces the SRs of all competing host SNNs slightly. We observe that the effectiveness of the SRM-based SNNs is dramatically impacted by the "GN weight" and "30% zero weight" pollution settings, especially the SAN. This means that SRM-based models are more sensitive to weight changes than LIF-based SNNs. Again, under the three degraded conditions, the proposed BDETT increases the SRs of the baseline model SAN-NR by at least 9.5%, 14.2%, and 14.8%. The success rates of the best and runner-up performers under "8-bit Loihi weight" and "30% zero weight" conditions are also qualitatively illustrated in Figure 3.

8

Table 1: Quantitative performance of obstacle avoidance with static obstacles.

Name	LIF ($T = 5$) SR↑	OTP	SRM ($T = 5$) SR↑	OTP	LIF ($T = 25$) SR↑	OTP	SRM ($T = 25$) SR↑	OTP
SAN	98%	0.0%	**96.5%**	0.0%	98%	0.0%	96%	0.0%
SAN-NR	98%	0.0%	95.5%	0.0%	**98.5%**	0.0%	95.5%	0.0%
DT1 [4]	96.5%	0.0%	95%	0.0%	96%	0.0%	94.5%	0.5%
DT2 [5]	97%	0.0%	95%	0.0%	97%	0.0%	94%	0.0%
DET only	96%	0.0%	95.5%	0.0%	95.5%	0.0%	95%	0.0%
DTT only	97%	0.0%	95.5%	0.0%	97%	0.0%	95%	0.0%
BDETT	**98.5%**	0.0%	**96.5%**	0.0%	98%	0.0%	**97%**	0.0%

Table 2: Quantitative performance of obstacle avoidance with dynamic obstacles.

Name	LIF ($T = 5$) SR↑	OTP	SRM ($T = 5$) SR↑	OTP	LIF ($T = 25$) SR↑	OTP	SRM ($T = 25$) SR↑	OTP
SAN	81.5%	0.0%	78.5%	0.0%	81%	0.0%	77.5%	0.0%
SAN-NR	83.5%	0.0%	77.5%	0.5%	83.5%	0.0%	77%	1.0%
DT1 [4]	74.5%	0.0%	68.5%	0.0%	74%	0.5%	68.5%	0.5%
DT2 [5]	80%	0.0%	71.5%	0.5%	80%	0.0%	71.5%	0.0%
DET only	81%	0.0%	78.5%	0.5%	80.5%	0.0%	78.5%	1.0%
DTT only	88%	0.0%	83.5%	0.0%	86.5%	0.0%	82%	0.0%
BDETT	**92.5%**	0.0%	**90.5%**	0.0%	**93%**	0.0%	**89.5%**	0.5%

Table 3: Quantitative performance of obstacle avoidance under degraded input conditions.

Type	Name	LIF ($T = 5$) SR↑	OTP	SRM ($T = 5$) SR↑	OTP	LIF ($T = 25$) SR↑	OTP	SRM ($T = 25$) SR↑	OTP
0.2	SAN	78.5%	1.5%	68%	1.0%	74%	2.5%	60.5%	1.0%
	SAN-NR	80%	2.5%	59%	3.0%	76%	3.0%	39.5%	4.5%
	DT1 [4]	65.5%	4.0%	64%	3.5%	60.5%	3.5%	58.5%	5.0%
	DT2 [5]	78%	3.0%	53.5%	3.5%	72.5%	4.0%	49%	3.5%
	DET only	83%	2.0%	71.5%	3.0%	77.5%	3.5%	67.5%	3.0%
	DTT only	78.5%	3.5%	64.5%	1.0%	72.5%	3.5%	62%	2.5%
	BDETT	**90%**	2.5%	**79.5%**	3.5%	**87.5%**	3.5%	**76%**	4.5%
6.0	SAN	71%	0.0%	70%	0.0%	73%	0.0%	72%	0.0%
	SAN-NR	70%	0.0%	61.5%	0.0%	71%	0.0%	65.5%	0.0%
	DT1 [4]	62%	0.0%	67%	0.0%	64%	0.0%	66.5%	0.0%
	DT2 [5]	61.5%	0.0%	55%	0.5%	61.5%	0.0%	57.5%	0.0%
	DET only	80%	0.0%	79%	0.0%	79.5%	0.0%	79.5%	0.0%
	DTT only	80%	0.0%	75.5%	0.0%	81%	0.0%	76%	0.0%
	BDETT	**84.5%**	0.0%	**83%**	0.0%	**86%**	0.0%	**83.5%**	0.0%
GN	SAN	71.5%	0.0%	57%	0.0%	63%	0.0%	51.5%	0.5%
	SAN-NR	72%	0.0%	65.5%	1.0%	67%	0.5%	54.5%	2.0%
	DT1 [4]	60.5%	0.5%	58%	0.0%	56.5%	0.5%	55.5%	0.0%
	DT2 [5]	71.5%	1.5%	61.5%	0.0%	68%	1.0%	57%	1.5%
	DET only	78.5%	1.0%	75.5%	0.5%	76%	2.0%	71%	0.5%
	DTT only	75.5%	0.0%	69%	0.0%	70.5%	0.0%	66.5%	0.5%
	BDETT	**84.5%**	0.0%	**82.5%**	0.0%	**81.5%**	0.0%	**79%**	0.5%

9
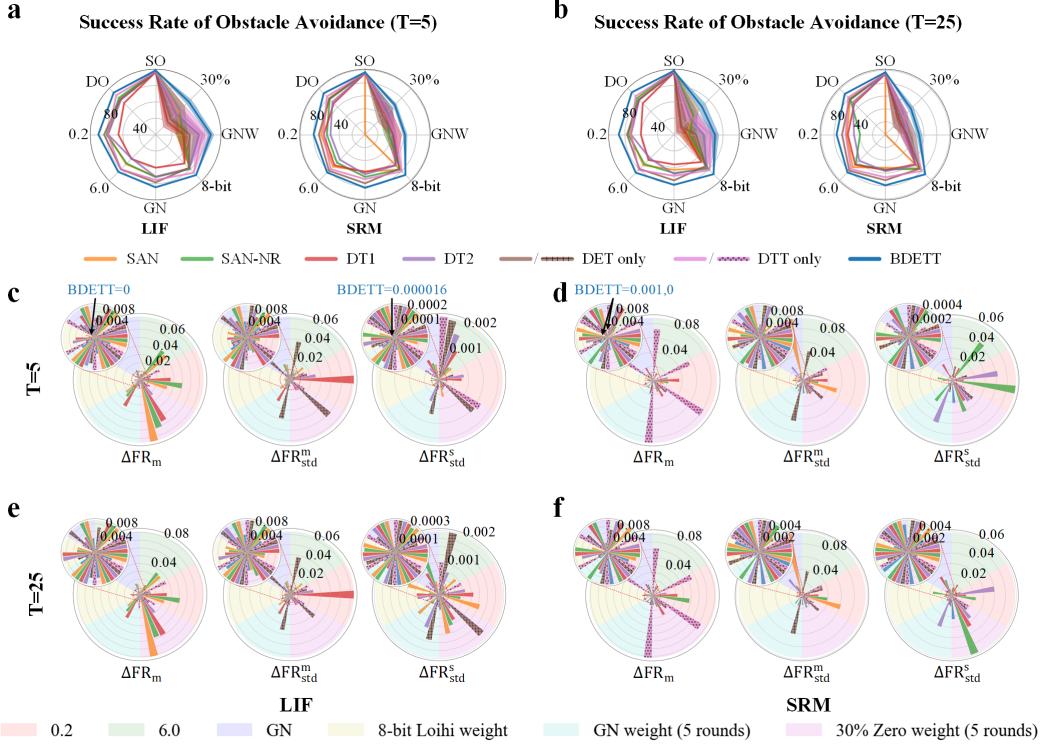
Figure 4: The experimental results obtained for the robot obstacle avoidance tasks. a & b. The SRs of obstacle avoidance under normal and different degraded conditions under the $T = 5$ and $T = 25$ settings, respectively. 'SO' denotes the static obstacle condition; 'DO' represents the dynamic obstacle condition; '0.2', '6.0', and 'GN' are the three degraded input conditions; '8-bit', 'GNW', and '30%' denotes the 8-bit Loihi weights, GN weights, and 30% zero weights, respectively. c & d. Homeostasis measurements obtained with the $T = 5$ setting by the LIF- and SRM-based host SNNs. e & f. The homeostasis results obtained with the $T = 25$ setup by the LIF- and SRM-based host SNNs, respectively.

Table 4: Quantitative performance of obstacle avoidance under weight uncertainty conditions.

Type	Name	**LIF** ($T = 5$)		**SRM** ($T = 5$)		**LIF** ($T = 25$)		**SRM** ($T = 25$)	
		SR↑	OTP	SR↑	OTP	SR↑	OTP	SR↑	OTP
8-bit Loihi weight	SAN	78.5%	0.0%	77%	0.0%	77.5%	0.0%	74.5%	0.0%
	SAN-NR	79.5%	0.0%	76.5%	0.5%	79%	0.0%	75.5%	0.0%
	DT1 [4]	70%	0.0%	67%	0.0%	67.5%	0.5%	65.5%	0.0%
	DT2 [5]	78.5%	0.0%	67.5%	1.0%	77%	0.0%	67%	0.5%
	DET only	77.5%	0.0%	75%	0.0%	74.5%	0.5%	75%	0.0%
	DTT only	86%	0.0%	80.5%	0.0%	81.5%	0.0%	80%	0.0%
	BDETT	**90%**	0.0%	**88.5%**	0.0%	**88.5%**	0.0%	**87.5%**	0.0%
GN weight (5 rounds)	SAN	51.3% (σ-6.8)	1.2%	0% (σ-0)	20.3%	36.2% (σ-7.3)	3.6%	0% (σ-0)	18.4%
	SAN-NR	52.5% (σ-7.1)	1.6%	37.2% (σ-7.6)	2.4%	39.0% (σ-7.8)	3.1%	38.4% (σ-8.9)	2.1%
	DT1 [4]	54.6% (σ-7.9)	2.3%	44.9% (σ-11.4)	3.0%	35.7% (σ-9.2)	3.3%	32.4% (σ-9.6)	4.7%
	DT2 [5]	73.2% (σ-7.4)	2.1%	43.6% (σ-4.4)	2.4%	56.2% (σ-9.3)	2.0%	30.3% (σ-5.7)	2.9%
	DET only	61.8% (σ-12.0)	1.8%	43.3% (σ-4.6)	2.5%	47.0% (σ-11.3)	2.3%	34.1% (σ-5.4)	2.6%
	DTT only	77.1% (σ-8.8)	1.5%	46.4% (σ-8.0)	1.6%	64.7% (σ-8.0)	1.8%	36.8% (σ-10.2)	1.4%
	BDETT	**87.7%** (σ-3.3)	0.8%	**61.8%** (σ-2.9)	1.3%	**70.1%** (σ-4.2)	0.4%	**52.6%** (σ-4.0)	2.5%
30% Zero weight (5 rounds)	SAN	59.3% (σ-10.5)	0.0%	0% (σ-0)	17.7%	51.2% (σ-11.3)	0.0%	0% (σ-0)	19.4%
	SAN-NR	61.6% (σ-7.5)	0.0%	46.5% (σ-12.4)	0.0%	53.6% (σ-6.7)	0.0%	36.5% (σ-9.9)	0.2%
	DT1 [4]	41.2% (σ-7.7)	0.7%	44.3% (σ-11.7)	0.0%	32.2% (σ-9.1)	1.3%	31.7% (σ-12.6)	0.6%
	DT2 [5]	55.6% (σ-9.3)	0.3%	49.1% (σ-10.8)	0.8%	48.0% (σ-10.5)	0.0%	37.8% (σ-10.2)	1.1%
	DET only	46.2% (σ-8.5)	0.0%	39.8% (σ-11.5)	1.4%	33.6% (σ-8.5)	0.8%	29.3% (σ-12.3)	2.5%
	DTT only	60.6% (σ-9.5)	0.0%	45.4% (σ-7.4)	0.5%	50.3% (σ-8.7)	0.4%	38.8% (σ-8.0)	1.3%
	BDETT	**77.2%** (σ-3.6)	0.0%	**65.2%** (σ-2.7)	0.3%	**68.4%** (σ-5.2)	0.0%	**56.5%** (σ-4.3)	0.7%

10

Table 5: The raw homeostasis measurements of successful trials and the corresponding changes with respect to the baseline condition in obstacle avoidance tasks with the $T = 5$ setting.

Type	Name	LIF ($T=5$)			SRM ($T=5$)		
		$\text{FR}_m(\Delta)$	$\text{FR}_{std}^m(\Delta)$	$\text{FR}_{std}^s(\Delta)$	$\text{FR}_m(\Delta)$	$\text{FR}_{std}^m(\Delta)$	$\text{FR}_{std}^s(\Delta)$
Dynamic obstacle (baseline condition)	SAN	0.523	0.325	0.000891	0.278	0.301	0.000596
	SAN-NR	0.515	0.330	0.001029	0.487	0.309	0.006853
	DT1 [4]	0.443	0.325	0.001738	0.482	0.310	0.002942
	DT2 [5]	0.400	0.345	0.002136	0.418	0.309	0.005873
	DET only	0.508	0.336	0.001024	0.380	0.276	0.002564
	DTT only	0.456	0.320	0.000902	0.475	0.294	0.002284
	BDETT	0.439	0.312	0.000916	0.501	0.298	0.001759
0.2	SAN	0.556 (0.033)	0.329 (0.004)	0.000750 (0.000141)	0.293 (0.015)	0.247 (0.054)	0.000746 (0.000150)
	SAN-NR	0.565 (0.050)	0.326 (0.004)	0.000738 (0.000291)	0.508 (0.021)	0.333 (0.024)	0.001069 (0.005784)
	DT1 [4]	0.479 (0.036)	0.387 (0.062)	0.000973 (0.000765)	0.518 (0.036)	0.348 (0.038)	0.003993 (0.001051)
	DT2 [5]	0.412 (0.012)	0.370 (0.025)	0.001293 (0.000843)	0.438 (0.020)	0.325 (0.016)	0.001709 (0.004164)
	DET only	0.495 (0.013)	0.353 (0.017)	0.001523 (0.000499)	0.380 (0.000)	0.244 (0.032)	0.003969 (0.001405)
	DTT only	0.481 (0.025)	0.335 (0.015)	0.000768 (0.000134)	0.420 (0.055)	0.335 (0.041)	0.002040 (0.000244)
	BDETT	0.444 (**0.005**)	0.315 (**0.003**)	0.000851 (**0.000065**)	0.494 (**0.007**)	0.310 (**0.012**)	0.001884 (**0.000125**)
6.0	SAN	0.564 (0.041)	0.342 (0.017)	0.001454 (0.000563)	0.275 (0.003)	0.306 (0.005)	0.000747 (0.000151)
	SAN-NR	0.558 (0.043)	0.339 (0.009)	0.001548 (0.000519)	0.483 (0.004)	0.306 (0.003)	0.002533 (0.004320)
	DT1 [4]	0.432 (0.011)	0.318 (0.007)	0.002862 (0.001124)	0.471 (0.011)	0.315 (0.005)	0.004224 (0.001282)
	DT2 [5]	0.407 (0.007)	0.354 (0.009)	0.003785 (0.001649)	0.408 (0.010)	0.320 (0.011)	0.005417 (0.000456)
	DET only	0.515 (0.007)	0.374 (0.038)	0.003088 (0.002064)	0.377 (0.003)	0.230 (0.046)	0.003889 (0.001325)
	DTT only	0.450 (0.006)	0.325 (0.005)	0.003057 (0.002155)	0.403 (0.072)	0.290 (0.004)	0.002855 (0.000571)
	BDETT	0.440 (**0.001**)	0.317 (**0.005**)	0.000960 (**0.000044**)	0.501 (**0.000**)	0.300 (**0.002**)	0.001870 (**0.000111**)
GN	SAN	0.534 (0.011)	0.310 (0.015)	0.001416 (0.000525)	0.287 (0.009)	0.204 (0.097)	0.000727 (0.000131)
	SAN-NR	0.527 (0.012)	0.314 (0.016)	0.001622 (0.000593)	0.497 (0.010)	0.298 (0.011)	0.007395 (0.000542)
	DT1 [4]	0.451 (0.008)	0.319 (0.006)	0.000982 (0.000756)	0.502 (0.020)	0.302 (0.008)	0.004634 (0.001692)
	DT2 [5]	0.405 (0.005)	0.337 (0.008)	0.001654 (0.000482)	0.423 (0.005)	0.283 (0.026)	0.005578 (0.000295)
	DET only	0.502 (0.006)	0.361 (0.025)	0.001228 (0.000204)	0.390 (0.010)	0.283 (0.007)	0.002454 (0.000110)
	DTT only	0.445 (0.011)	0.315 (0.005)	0.001453 (0.000551)	0.390 (0.085)	0.308 (0.014)	0.001968 (0.000316)
	BDETT	0.443 (**0.004**)	0.307 (**0.005**)	0.000880 (**0.000036**)	0.500 (**0.001**)	0.301 (**0.003**)	0.001886 (**0.000127**)
8-bit Loihi weight	SAN	0.520 (0.003)	0.319 (0.006)	0.000988 (0.000097)	0.288 (0.010)	0.314 (0.013)	0.000731 (**0.000135**)
	SAN-NR	0.513 (0.002)	0.334 (**0.004**)	0.001286 (0.000257)	0.479 (0.008)	0.315 (0.006)	0.005527 (0.001326)
	DT1 [4]	0.437 (0.006)	0.319 (0.006)	0.001589 (0.000149)	0.473 (0.009)	0.325 (0.015)	0.002084 (0.000858)
	DT2 [5]	0.407 (0.005)	0.340 (0.005)	0.001853 (0.000283)	0.425 (0.007)	0.316 (0.007)	0.005638 (0.000235)
	DET only	0.505 (0.003)	0.341 (0.005)	0.000868 (0.000156)	0.385 (0.005)	0.285 (0.009)	0.002185 (0.000379)
	DTT only	0.446 (0.010)	0.325 (0.005)	0.000787 (0.000115)	0.460 (0.015)	0.301 (0.007)	0.002436 (0.000152)
	BDETT	0.439 (**0.000**)	0.308 (**0.004**)	0.000932 (**0.000016**)	0.500 (**0.001**)	0.293 (**0.005**)	0.001570 (0.000189)
GN weight (5 rounds)	SAN	0.501 (0.022)	0.338 (0.013)	0.001192 (0.000301)	-	-	-
	SAN-NR	0.490 (0.025)	0.338 (0.008)	0.001281 (0.000252)	0.498 (0.011)	0.326 (0.017)	0.004461 (0.002392)
	DT1 [4]	0.407 (0.036)	0.349 (0.024)	0.001902 (0.000164)	0.487 (0.005)	0.319 (0.009)	0.003573 (0.000631)
	DT2 [5]	0.391 (0.009)	0.335 (0.010)	0.001356 (0.000780)	0.410 (0.008)	0.291 (0.018)	0.010002 (0.004129)
	DET only	0.516 (0.008)	0.375 (0.039)	0.002225 (0.001201)	0.399 (0.019)	0.212 (0.064)	0.003675 (0.001111)
	DTT only	0.467 (0.011)	0.327 (0.007)	0.001244 (0.000342)	0.387 (0.088)	0.301 (0.007)	0.002387 (0.000103)
	BDETT	0.444 (**0.005**)	0.318 (**0.006**)	0.001013 (**0.000097**)	0.498 (**0.003**)	0.299 (**0.001**)	0.001602 (**0.000157**)
30% Zero weight (5 rounds)	SAN	0.448 (0.075)	0.321 (**0.004**)	0.001490 (0.000599)	-	-	-
	SAN-NR	0.454 (0.061)	0.335 (0.005)	0.001399 (0.000370)	0.470 (0.017)	0.331 (0.022)	0.009941 (0.003088)
	DT1 [4]	0.387 (0.056)	0.313 (0.012)	0.002045 (0.000307)	0.456 (0.026)	0.334 (0.024)	0.005103 (0.002161)
	DT2 [5]	0.377 (0.023)	0.358 (0.013)	0.001834 (0.000302)	0.403 (0.015)	0.332 (0.023)	0.003469 (0.002404)
	DET only	0.520 (0.012)	0.387 (0.051)	0.002582 (0.001558)	0.356 (0.024)	0.235 (0.041)	0.005036 (0.002472)
	DTT only	0.470 (0.014)	0.337 (0.017)	0.002551 (0.001649)	0.394 (0.081)	0.274 (0.020)	0.003706 (0.001422)
	BDETT	0.444 (**0.005**)	0.316 (**0.004**)	0.000993 (**0.000077**)	0.497 (**0.004**)	0.318 (**0.020**)	0.003855 (**0.002096**)

Assessment—Homeostatic

In the main manuscript, we show the quantified homeostasis changes induced during all successful trials with respect to the base condition (the homeostasis obtained in the dynamic obstacle experiments) under the $T = 5$ setting. Table 5 provides the raw homeostasis measurements and the corresponding changes used for plotting the polar chart in the main manuscript.

We also offer the measured homeostasis and corresponding changes obtained under the $T = 25$ setting in Table 6. The corresponding polar plots are shown in Figures 4e and f. Similar to the observations obtained in the experiments with $T = 5$, the association between homeostasis and the obstacle avoidance SR still holds for $T = 25$; stronger homeostasis offers better performance. Notably, our approach induces the smallest changes in the three metrics across all experimental settings, except for the FR_{std}^m obtained in the SRM-based 8-bit Loihi weight experiment. Furthermore, the proposed BDETT delivers the best obstacle avoidance SRs in all designed experimental conditions with $T = 25$; see Tables 2, 3, and 4 and Figures 4e and f.

11

Table 6: The raw homeostasis measurements of successful trials and the corresponding changes with respect to the baseline condition in obstacle avoidance tasks with the $T = 25$ setting.

Type	Name	LIF ($T = 25$)			SRM ($T = 25$)		
		$\text{FR}_m(\Delta)$	$\text{FR}^m_{std}(\Delta)$	$\text{FR}^s_{std}(\Delta)$	$\text{FR}_m(\Delta)$	$\text{FR}^m_{std}(\Delta)$	$\text{FR}^s_{std}(\Delta)$
Dynamic obstacle (baseline condition)	SAN	0.524	0.325	0.002098	0.285	0.306	0.001504
	SAN-NR	0.515	0.331	0.001440	0.488	0.312	0.003486
	DT1 [4]	0.447	0.324	0.002155	0.485	0.319	0.002473
	DT2 [5]	0.401	0.347	0.002470	0.420	0.314	0.005771
	DET only	0.509	0.336	0.001206	0.384	0.279	0.002483
	DTT only	0.449	0.317	0.001736	0.475	0.301	0.002515
	BDETT	0.439	0.311	0.001035	0.501	0.301	0.002394
0.2	SAN	0.556 (0.032)	0.330 (0.005)	0.000798 (0.001300)	0.294 (0.009)	0.245 (0.061)	0.001004 (0.000500)
	SAN-NR	0.566 (0.051)	0.326 (0.005)	0.000768 (0.000670)	0.536 (0.048)	0.351 (0.039)	0.001224 (0.002260)
	DT1 [4]	0.481 (0.034)	0.387 (0.063)	0.001097 (0.001060)	0.517 (0.032)	0.344 (0.025)	0.003823 (0.001350)
	DT2 [5]	0.415 (0.014)	0.370 (0.023)	0.001662 (0.000810)	0.438 (0.018)	0.326 (0.012)	0.001781 (0.003990)
	DET only	0.496 (0.013)	0.353 (0.017)	0.001424 (0.000218)	0.380 (0.004)	0.246 (0.033)	0.003362 (0.000879)
	DTT only	0.485 (0.036)	0.336 (0.019)	0.000972 (0.000760)	0.420 (0.055)	0.335 (0.034)	0.003116 (0.000601)
	BDETT	0.444 (**0.005**)	0.314 (**0.003**)	0.001104 (**0.000069**)	0.494 (**0.007**)	0.310 (**0.010**)	0.002238 (**0.000160**)
6.0	SAN	0.558 (0.034)	0.341 (0.016)	0.001415 (0.000683)	0.275 (0.010)	0.303 (0.003)	0.000839 (0.000665)
	SAN-NR	0.550 (0.035)	0.340 (0.009)	0.001165 (0.000275)	0.484 (0.004)	0.306 (0.006)	0.003828 (0.000342)
	DT1 [4]	0.433 (0.014)	0.319 (**0.005**)	0.002449 (0.000294)	0.471 (0.014)	0.315 (0.004)	0.003621 (0.001148)
	DT2 [5]	0.406 (0.005)	0.353 (0.006)	0.003206 (0.000736)	0.406 (0.014)	0.320 (0.006)	0.005094 (0.000667)
	DET only	0.516 (0.007)	0.374 (0.038)	0.003172 (0.001966)	0.377 (0.007)	0.241 (0.038)	0.003248 (0.000765)
	DTT only	0.450 (0.001)	0.327 (0.010)	0.002744 (0.001008)	0.413 (0.062)	0.289 (0.012)	0.002742 (0.000227)
	BDETT	0.440 (**0.001**)	0.316 (**0.005**)	0.001247 (**0.000212**)	0.501 (**0.000**)	0.300 (**0.001**)	0.002092 (**0.000302**)
GN	SAN	0.538 (0.014)	0.311 (0.014)	0.002522 (0.000424)	0.288 (0.003)	0.209 (0.097)	0.000883 (0.000621)
	SAN-NR	0.530 (0.015)	0.318 (0.013)	0.003055 (0.001615)	0.503 (0.015)	0.299 (0.013)	0.005029 (0.001543)
	DT1 [4]	0.452 (0.005)	0.319 (**0.005**)	0.001408 (0.000747)	0.502 (0.017)	0.302 (0.017)	0.004470 (0.001997)
	DT2 [5]	0.405 (**0.004**)	0.336 (0.011)	0.002005 (0.000465)	0.423 (**0.003**)	0.283 (0.031)	0.005235 (0.000536)
	DET only	0.500 (0.009)	0.367 (0.031)	0.001424 (0.000218)	0.392 (0.008)	0.286 (0.007)	0.003130 (0.000647)
	DTT only	0.445 (0.004)	0.311 (0.006)	0.001260 (0.000476)	0.401 (0.074)	0.310 (0.009)	0.001795 (0.000720)
	BDETT	0.443 (0.004)	0.306 (**0.005**)	0.001085 (**0.000050**)	0.498 (0.003)	0.301 (**0.000**)	0.001962 (**0.000432**)
8-bit Loihi weight	SAN	0.519 (0.005)	0.319 (0.006)	0.001106 (0.000992)	0.290 (0.005)	0.315 (0.009)	0.000961 (0.000543)
	SAN-NR	0.510 (0.005)	0.336 (0.005)	0.001153 (0.000287)	0.478 (0.010)	0.317 (0.005)	0.005220 (0.001734)
	DT1 [4]	0.435 (0.012)	0.318 (0.006)	0.001467 (0.000688)	0.472 (0.013)	0.327 (0.008)	0.001854 (0.000619)
	DT2 [5]	0.411 (0.010)	0.339 (0.008)	0.001802 (0.000668)	0.428 (0.008)	0.317 (**0.003**)	0.005032 (0.000739)
	DET only	0.504 (0.005)	0.341 (0.005)	0.000924 (0.000282)	0.387 (0.003)	0.288 (0.009)	0.002816 (0.000333)
	DTT only	0.446 (0.003)	0.327 (0.010)	0.001302 (0.000434)	0.462 (0.013)	0.303 (0.002)	0.002038 (0.000477)
	BDETT	0.439 (**0.000**)	0.308 (**0.003**)	0.001107 (**0.000072**)	0.502 (0.001)	0.297 (0.004)	0.002164 (**0.000230**)
GN weight (5 rounds)	SAN	0.503 (0.021)	0.340 (0.015)	0.001241 (0.000857)	-	-	-
	SAN-NR	0.488 (0.027)	0.340 (0.009)	0.001796 (0.000356)	0.499 (0.011)	0.328 (0.016)	0.004204 (0.000718)
	DT1 [4]	0.413 (0.034)	0.346 (0.022)	0.002318 (0.000163)	0.491 (0.006)	0.320 (**0.001**)	0.003065 (0.000592)
	DT2 [5]	0.390 (0.011)	0.336 (0.011)	0.001382 (0.001088)	0.411 (0.007)	0.292 (0.017)	0.008895 (0.003124)
	DET only	0.516 (0.007)	0.372 (0.036)	0.002643 (0.001437)	0.397 (0.013)	0.218 (0.061)	0.003384 (0.000901)
	DTT only	0.467 (0.018)	0.328 (0.011)	0.001352 (0.000384)	0.393 (0.082)	0.303 (0.002)	0.003581 (0.001066)
	BDETT	0.444 (**0.005**)	0.318 (**0.007**)	0.001163 (**0.000128**)	0.498 (**0.003**)	0.300 (**0.001**)	0.001923 (**0.000471**)
30% Zero weight (5 rounds)	SAN	0.443 (0.081)	0.320 (**0.005**)	0.000862 (0.001236)	-	-	-
	SAN-NR	0.457 (0.058)	0.338 (0.007)	0.002461 (0.001021)	0.472 (0.016)	0.332 (0.020)	0.009380 (0.005894)
	DT1 [4]	0.388 (0.059)	0.312 (0.012)	0.001257 (0.000898)	0.456 (0.029)	0.334 (**0.015**)	0.005820 (0.003347)
	DT2 [5]	0.372 (0.029)	0.359 (0.012)	0.001930 (0.000540)	0.403 (0.017)	0.332 (0.018)	0.003060 (0.002711)
	DET only	0.524 (0.015)	0.368 (0.032)	0.002974 (0.001786)	0.360 (0.024)	0.245 (0.034)	0.004378 (0.001895)
	DTT only	0.472 (0.023)	0.334 (0.017)	0.002013 (0.000277)	0.402 (0.073)	0.280 (0.021)	0.004420 (0.001905)
	BDETT	0.446 (**0.007**)	0.316 (**0.005**)	0.001502 (**0.000467**)	0.488 (**0.013**)	0.316 (**0.015**)	0.004638 (**0.002244**)

Assessment—Ablation Studies

We conduct ablation studies to validate the effectiveness of the DET and DTT components of the proposed BDETT. The results obtained under different degraded conditions are reported in the rows named "DET only" and "DTT only" in Tables 1, 2, 3, and 4. The ablation study results are also illustrated in Figure 4. All listed evaluations validate that the BDETT scheme performs better than any single component. The dynamic threshold scheme with only one component cannot effectively regulate the firing rate statuses of the host SNNs, prohibiting meaningful homeostasis. One extreme example is illustrated in Figure 4f. The ΔFR_m changes induced under the 'DTT only' setting are the largest among all competing approaches under all experimental conditions. Notably, when combined with the other component, the proposed BDETT provides the strongest homeostasis for the host SNNs. This validates the biologically observed positive correlation encoded by the DET and the negative correlation enforced by the DTT, which are equally essential for effectively maintaining the homeostasis of an SNN.

12

Supplementary Note 5: Additional Details on Continuous Control Experiments—HalfCheetah-v3

Training

The adopted population-coded SAN (PopSAN) and its modified variants are trained by using the twin-delayed deep deterministic policy gradient (TD3) off-policy algorithm [25] and the following hyperparameter settings: $D = 0.75$ for the LIF; $\eta = 0.01$ and $\psi = 6.0$ for the DET; $C = 3.0$ for the DTT; and $\tau_s = \tau_r = 1.0$ for the SRM. Compared to the settings of the obstacle avoidance tasks, the only different setting is the value of ψ for the DET. Following the training protocol of the PopSAN, we set the batch size to 100 and the learning rates to 0.0001 for both the actor and critic networks. The reward discount factor is set to 0.99, and the maximum length of the replay buffer is set to 1 million. We use PyTorch [23] to train all competing SNNs with an i7-7700 CPU and an NVIDIA GTX 1080Ti GPU.
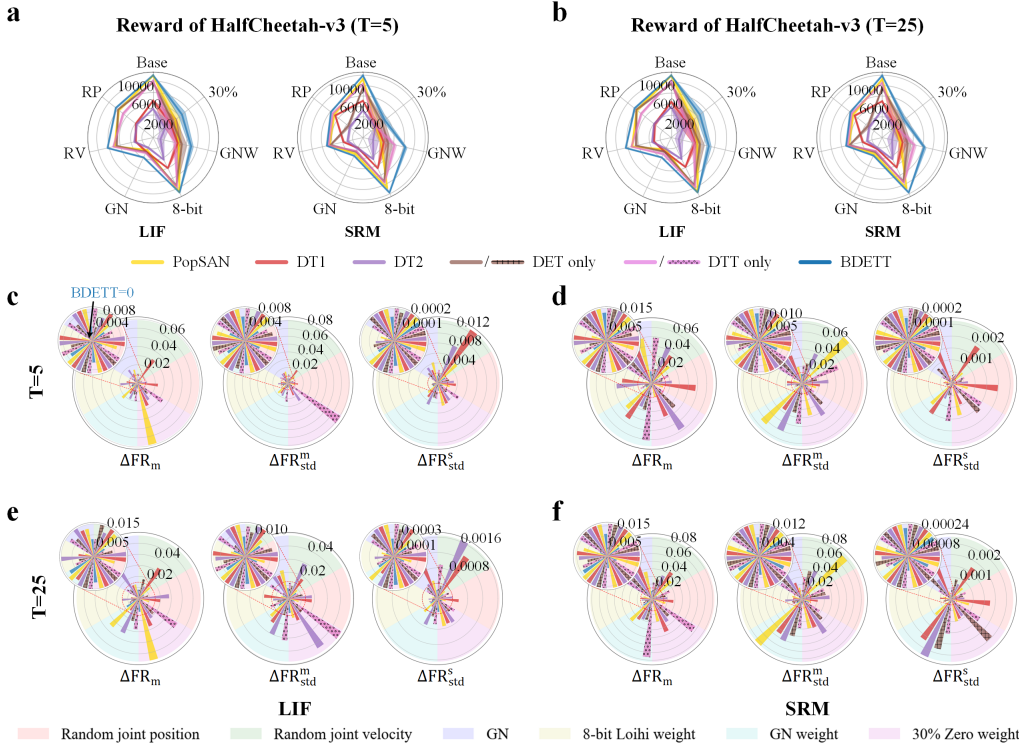
Figure 5: The experimental results obtained in the HalfCheetah-v3 tasks. a & b. The rewards obtained under normal and different degraded conditions with $T = 5$ and $T = 25$ settings, respectively. 'Base' indicates the base condition; 'RP' indicates random joint position; 'RV' denotes random joint velocity; '8-bit', 'GNW', and '30%' denote the 8-bit Loihi weights, GN weights, and 30% zero weights, respectively. c & d. Homeostasis measurements obtained with the $T = 5$ setting for the LIF- and SRM-based host SNNs, respectively. e & f. Homeostasis results obtained with the $T = 25$ setup for the LIF- and SRM-based host SNNs, respectively.

Assessment—Reward

After determining the evaluation settings of the PopSAN [26], we train ten models corresponding to ten random seeds, and the best-performing model is used for our assessments under different degraded conditions. In particular, the best-performing model is evaluated ten times under each experimental condition, and the mean reward of the ten evaluations represents the model's performance. Each evaluation consists of ten episodes, and each episode lasts for a maximum of 1000 execution steps. Table 7 shows the ten evaluations' average rewards and the corresponding standard deviations of all competing SNNs under a normal testing condition. Here, we also present the quantitative performance

13

Table 7: Quantitative Performance of Mujoco HalfCheetah-v3 Tasks under standard testing condition.

	LIF ($T = 5$)	**SRM** ($T = 5$)	**LIF** ($T = 25$)	**SRM** ($T = 25$)
Name	Reward↑	Reward↑	Reward↑	Reward↑
PopSAN	10989 (σ-49)	11268 (σ-149)	11137 (σ-70)	11247 (σ-132)
DT1 [4]	6572 (σ-85)	7085 (σ-69)	6438 (σ-102)	7001 (σ-82)
DT2 [5]	5110 (σ-30)	5262 (σ-77)	5523 (σ-67)	5311 (σ-113)
DET only	9794 (σ-107)	9694 (σ-112)	9704 (σ-125)	9619 (σ-105)
DTT only	10104 (σ-44)	10332 (σ-106)	10221 (σ-57)	10563 (σ-83)
BDETT	**11064** (σ-28)	**11960** (σ-86)	**11209** (σ-56)	**11956** (σ-95)

achieved under the $T = 5$ and $T = 25$ settings. With both the LIF and SRM models, the proposed BDETT offers the host SNNs the best rewards in all experimental settings under normal testing conditions (the base conditions).

Unlike in the obstacle avoidance tasks, even with grid searches, the rewards offered by DT1 and DT2 are significantly lower than those provided by the baseline PopSAN model. This indicates that dynamic threshold schemes may perform worse than a simple static threshold, especially for heuristic-based schemes. More importantly, we observe similar patterns in the obstacle avoidance tasks; the SRs offered by DT1 and DT2 are lower than those of the baseline SAN-NR model in most experimental conditions.

Tables 8 and 9 show the quantitative performance of all competing approaches under degraded input and weight uncertainty conditions, respectively. The results are also illustrated in Figures 5a and b for the $T = 5$ and $T = 25$ settings, respectively. We provide a more detailed analysis for each degraded condition in the following.

Degraded Inputs In the HalfCheetah-v3 continuous control task, an observation (state) s represents 17-dimensional data consisting of 8-dimensional joint position information and 9-dimensional joint velocity information. Similar to the degraded input experiments conducted in the robot obstacle avoidance tasks, we disturb a HalfCheetah-v3's observations in three different ways. a) "Random joint position": for each episode, one of the eight joint positions is randomly selected, and its original position is replaced by a random number sampled from a Gaussian distribution $\mathcal{N}(0, 0.1)$. b) "Random joint velocity": we randomly select one of the nine joint velocities in each episode and change its observed velocity to a random number sampled from a Gaussian distribution $\mathcal{N}(0, 10.0)$. c) "GN": For each episode, we add Gaussian noise ($s_{input} + \mathcal{N}(0, 1.0)$, as suggested in a study regarding LSTM-LMC [24]) to each of the 17 joint states. The average rewards obtained from the ten evaluations conducted under these three different conditions are shown in Table 8.

Under all experimental settings, the proposed BDETT offers the host SNNs the highest rewards, significantly improving upon the rewards of the baseline PopSAN model by at least 438 with $T = 5$, and 358 with $T = 25$. Compared to the other two degraded input conditions, the "GN" condition disturbs all dimensions of the HalfCheetah-v3 state. Therefore, we observe that the lowest rewards obtained by all host SNNs occur with the "GN" setting. Even though the DT1 method hosted by an LIF-based SNN reduces the rewards of the baseline PopSAN model by almost half, it outperforms the baseline model with both T settings under the "GN" condition. Furthermore, the proposed BDETT provides the most stable performance, highlighted by it obtaining the smallest standard deviations under all the degraded input settings.

Weight Uncertainty We leverage the same weight uncertainty conditions as those introduced in robot obstacle avoidance experiments to demonstrate the effectiveness of all competing dynamic threshold schemes, and the corresponding results are shown in Table 9. The proposed BDETT remains the best performer under the weight uncertainty conditions. Note that the SRM-based BDETT outperforms other methods by significant margins under the "GN weight" settings, highlighting that the proposed dynamic threshold scheme can effectively deal with weight uncertainty errors. We also notice that the DT2 scheme produces the lowest rewards under all experimental weight uncertainty settings, indicating that predefining a target firing rate does not work well with weight uncertainty conditions. Surprisingly, even with low-precision 8-bit weights, the proposed BDETT helps the SRM-based host SNN achieve higher rewards than those obtained with high-precision weights under the $T = 5$ and $T = 25$ settings (11767 vs. 11268 with $T = 5$ and 11760 vs. 11247 with $T = 25$).

14

Table 8: Quantitative performance of Mujoco HalfCheetah-v3 tasks under degraded input conditions.

Type	Name	**LIF** ($T = 5$) Reward↑	**SRM** ($T = 5$) Reward↑	**LIF** ($T = 25$) Reward↑	**SRM** ($T = 25$) Reward↑
Random joint position	PopSAN	7832 (σ-222)	7120 (σ-214)	7947 (σ-253)	7167 (σ-197)
	DT1 [4]	3923 (σ-204)	6830 (σ-140)	3835 (σ-248)	6792 (σ-157)
	DT2 [5]	3750 (σ-171)	3230 (σ-239)	3950 (σ-192)	3213 (σ-230)
	DET only	7954 (σ-103)	3582 (σ-284)	8051 (σ-148)	3502 (σ-323)
	DTT only	6817 (σ-221)	7428 (σ-234)	6922 (σ-202)	7493 (σ-182)
	BDETT	**8465** (σ-121)	**7883** (σ-78)	**8463** (σ-130)	**7846** (σ-70)
Random joint velocity	PopSAN	7020 (σ-146)	6576 (σ-147)	7223 (σ-165)	6583 (σ-168)
	DT1 [4]	3187 (σ-142)	3836 (σ-181)	3203 (σ-148)	3855 (σ-202)
	DT2 [5]	3395 (σ-209)	3031 (σ-239)	3506 (σ-208)	2965 (σ-241)
	DET only	6664 (σ-179)	6392 (σ-206)	6498 (σ-219)	6435 (σ-213)
	DTT only	7249 (σ-137)	6772 (σ-299)	7363 (σ-150)	6762 (σ-247)
	BDETT	**8302** (σ-84)	**7116** (σ-146)	**8422** (σ-94)	**7127** (σ-131)
GN	PopSAN	2440 (σ-199)	3457 (σ-187)	2393 (σ-214)	3494 (σ-187)
	DT1 [4]	2790 (σ-187)	2210 (σ-124)	2773 (σ-198)	2355 (σ-120)
	DT2 [5]	1994 (σ-175)	2307 (σ-272)	2281 (σ-223)	2210 (σ-251)
	DET only	2831 (σ-157)	3013 (σ-130)	2807 (σ-163)	3061 (σ-155)
	DTT only	2974 (σ-194)	2851 (σ-81)	3281 (σ-173)	2855 (σ-115)
	BDETT	**3909** (σ-101)	**3895** (σ-81)	**3965** (σ-83)	**3852** (σ-69)

Table 9: Quantitative performance of Mujoco HalfCheetah-v3 tasks under weight uncertainty conditions.

Type	Name	**LIF** ($T = 5$) Reward↑	**SRM** ($T = 5$) Reward↑	**LIF** ($T = 25$) Reward↑	**SRM** ($T = 25$) Reward↑
8-bit Loihi weight	PopSAN	10728 (σ-47)	10802 (σ-32)	10926 (σ-59)	10850 (σ-44)
	DT1 [4]	6026 (σ-63)	6569 (σ-46)	5883 (σ-102)	6420 (σ-97)
	DT2 [5]	4372 (σ-54)	4629 (σ-50)	4301 (σ-87)	4636 (σ-74)
	DET only	9455 (σ-125)	9398 (σ-60)	9474 (σ-137)	9376 (σ-82)
	DTT only	9803 (σ-44)	9636 (σ-84)	9968 (σ-69)	9645 (σ-113)
	BDETT	**10823** (σ-37)	**11767** (σ-45)	**10990** (σ-61)	**11760** (σ-68)
GN weight	PopSAN	4640 (σ-510)	3583 (σ-347)	4816 (σ-583)	3597 (σ-426)
	DT1 [4]	4483 (σ-491)	4128 (σ-754)	4365 (σ-466)	4051 (σ-760)
	DT2 [5]	1334 (σ-616)	2028 (σ-1026)	1402 (σ-721)	1982 (σ-993)
	DET only	5251 (σ-859)	5032 (σ-705)	5313 (σ-801)	5035 (σ-652)
	DTT only	4013 (σ-423)	6250 (σ-368)	4238 (σ-468)	6327 (σ-403)
	BDETT	**6928** (σ-373)	**8381** (σ-320)	**6957** (σ-429)	**8321** (σ-352)
30% Zero weight	PopSAN	5020 (σ-923)	3233 (σ-879)	5078 (σ-1031)	3304 (σ-950)
	DT1 [4]	3995 (σ-1319)	3503 (σ-571)	3927 (σ-1406)	3484 (σ-772)
	DT2 [5]	2721 (σ-1281)	3056 (σ-555)	2713 (σ-1352)	3002 (σ-582)
	DET only	4436 (σ-801)	4682 (σ-540)	4406 (σ-822)	4692 (σ-515)
	DTT only	3583 (σ-692)	3268 (σ-641)	3604 (σ-662)	3359 (σ-705)
	BDETT	**6551** (σ-679)	**5386** (σ-443)	**6619** (σ-712)	**5474** (σ-388)

Assessment—Homeostatic

In the main manuscript, the changes in the quantified homeostasis values with respect to the base condition (the normal Mujoco testing condition) under $T = 5$ are illustrated. The raw homeostasis measurements and the corresponding changes used for plotting the polar chart in the main manuscript are reported in Table 10. In addition, we also provide the experimental homeostasis results obtained under $T = 25$ in Table 11. The corresponding polar plots obtained under the $T = 5$ and $T = 25$ setups are shown in Figures 5c-f.

The results are consistent with those obtained in the obstacle avoidance tasks. The proposed BDETT scheme offers the strongest homeostasis, indicating the effectiveness of the proposed dynamic threshold scheme. The essential goal of homeostasis is to enhance the host SNN's performance. Therefore, we expect the SNNs with stronger homeostasis (smaller ΔFR_m, ΔFR^m_{std}, and ΔFR^s_{std} values) to outperform those with weaker homeostasis. Our experimental results confirm this expectation.

15

Table 10: The raw homeostasis measurements and the corresponding changes with respect to the baseline condition in Mujoco HalfCheetah-v3 tasks with $T = 5$.

Type	Name	LIF ($T=5$)			SRM ($T=5$)		
		$FR_m(\Delta)$	$FR_{std}^m(\Delta)$	$FR_{std}^s(\Delta)$	$FR_m(\Delta)$	$FR_{std}^m(\Delta)$	$FR_{std}^s(\Delta)$
baseline condition	PopSAN	0.433	0.228	0.000978	0.427	0.241	0.002146
	DT1 [4]	0.412	0.239	0.001342	0.474	0.248	0.002166
	DT2 [5]	0.697	0.298	0.000911	0.530	0.302	0.001472
	DET only	0.284	0.220	0.001084	0.335	0.243	0.001558
	DTT only	0.646	0.257	0.002291	0.501	0.334	0.002541
	BDETT	0.249	0.190	0.001152	0.212	0.160	0.000952
Random joint position	PopSAN	0.426 (0.007)	0.237 (0.009)	0.001230 (0.000252)	0.440 (0.013)	0.258 (0.017)	0.002852 (0.000706)
	DT1 [4]	0.435 (0.023)	0.252 (0.013)	0.001713 (0.000371)	0.426 (0.048)	0.269 (0.021)	0.004145 (0.001979)
	DT2 [5]	0.686 (0.011)	0.289 (0.009)	0.001239 (0.000328)	0.508 (0.022)	0.333 (0.031)	0.002164 (0.000692)
	DET only	0.289 (0.005)	0.227 (0.007)	0.001323 (0.000239)	0.347 (0.012)	0.261 (0.018)	0.002006 (0.000448)
	DTT only	0.640 (0.006)	0.263 (0.006)	0.002077 (0.000214)	0.521 (0.020)	0.380 (0.046)	0.003124 (0.000583)
	BDETT	0.246 (**0.003**)	0.186 (**0.004**)	0.001268 (**0.000116**)	0.209 (**0.003**)	0.152 (**0.008**)	0.001071 (**0.000119**)
Random joint velocity	PopSAN	0.439 (0.006)	0.240 (0.012)	0.001502 (0.000524)	0.453 (0.026)	0.314 (0.073)	0.001513 (0.000633)
	DT1 [4]	0.381 (0.031)	0.259 (0.020)	0.002602 (0.001260)	0.510 (0.036)	0.261 (0.013)	0.004051 (0.001885)
	DT2 [5]	0.690 (0.007)	0.289 (0.009)	0.001725 (0.000814)	0.487 (0.043)	0.340 (0.038)	0.001896 (0.000424)
	DET only	0.280 (**0.004**)	0.214 (0.006)	0.000905 (**0.000179**)	0.351 (0.016)	0.219 (0.024)	0.001846 (0.000288)
	DTT only	0.656 (0.010)	0.246 (0.011)	0.002027 (0.000264)	0.550 (0.049)	0.355 (0.021)	0.002891 (0.000350)
	BDETT	0.245 (**0.004**)	0.186 (**0.004**)	0.001336 (0.000184)	0.204 (**0.008**)	0.168 (**0.008**)	0.001104 (**0.000152**)
GN	PopSAN	0.418 (0.015)	0.243 (0.015)	0.001400 (0.000422)	0.476 (0.049)	0.221 (0.020)	0.002481 (0.000335)
	DT1 [4]	0.423 (0.011)	0.225 (0.014)	0.001623 (0.000281)	0.535 (0.061)	0.283 (0.035)	0.004810 (0.002644)
	DT2 [5]	0.680 (0.017)	0.312 (0.014)	0.001273 (0.000362)	0.481 (0.049)	0.362 (0.060)	0.002215 (0.000743)
	DET only	0.278 (0.006)	0.212 (0.008)	0.001353 (0.000269)	0.302 (0.033)	0.277 (0.034)	0.002411 (0.000853)
	DTT only	0.638 (0.008)	0.269 (0.012)	0.002448 (0.000157)	0.434 (0.067)	0.301 (0.033)	0.002062 (0.000479)
	BDETT	0.245 (**0.004**)	0.184 (**0.006**)	0.001300 (**0.000148**)	0.225 (**0.013**)	0.171 (**0.011**)	0.001093 (**0.000141**)
8-bit Loihi weight	PopSAN	0.430 (0.003)	0.221 (0.007)	0.001061 (0.000083)	0.420 (0.007)	0.252 (0.011)	0.001847 (0.000299)
	DT1 [4]	0.424 (0.012)	0.248 (0.009)	0.001285 (0.000057)	0.442 (0.032)	0.230 (0.018)	0.002520 (0.000354)
	DT2 [5]	0.678 (0.019)	0.285 (0.013)	0.001022 (0.000111)	0.492 (0.038)	0.320 (0.018)	0.001701 (0.000229)
	DET only	0.290 (0.006)	0.229 (0.009)	0.001211 (0.000127)	0.327 (0.008)	0.235 (0.008)	0.001303 (0.000255)
	DTT only	0.655 (0.009)	0.264 (0.007)	0.002402 (0.000111)	0.488 (0.013)	0.343 (0.009)	0.002707 (0.000166)
	BDETT	0.249 (**0.000**)	0.186 (**0.004**)	0.001114 (**0.000038**)	0.215 (**0.003**)	0.163 (**0.003**)	0.000907 (**0.000045**)
GN weight	PopSAN	0.456 (0.023)	0.210 (0.018)	0.001249 (0.000271)	0.464 (0.037)	0.305 (0.064)	0.003358 (0.001212)
	DT1 [4]	0.426 (0.014)	0.223 (0.016)	0.001004 (0.000338)	0.429 (0.045)	0.285 (0.037)	0.003702 (0.001536)
	DT2 [5]	0.678 (0.019)	0.316 (0.018)	0.001381 (0.000470)	0.503 (0.027)	0.362 (0.060)	0.002172 (0.000700)
	DET only	0.271 (0.013)	0.227 (0.007)	0.001385 (0.000301)	0.364 (0.029)	0.208 (0.035)	0.001042 (0.000516)
	DTT only	0.626 (0.020)	0.281 (0.024)	0.001972 (0.000319)	0.562 (0.061)	0.287 (0.047)	0.004133 (0.001592)
	BDETT	0.256 (**0.007**)	0.185 (**0.005**)	0.001264 (**0.000112**)	0.219 (**0.007**)	0.165 (**0.005**)	0.001049 (**0.000097**)
30% Zero weight	PopSAN	0.502 (0.069)	0.220 (0.008)	0.001441 (0.000463)	0.412 (0.015)	0.279 (0.038)	0.003522 (0.001376)
	DT1 [4]	0.439 (0.027)	0.256 (0.017)	0.001784 (0.000442)	0.436 (0.038)	0.263 (0.015)	0.001216 (0.000950)
	DT2 [5]	0.675 (0.022)	0.325 (0.027)	0.001327 (0.000416)	0.472 (0.058)	0.258 (0.044)	0.000994 (0.000478)
	DET only	0.268 (0.016)	0.210 (0.010)	0.001329 (0.000245)	0.370 (0.035)	0.210 (0.033)	0.003205 (0.001647)
	DTT only	0.680 (0.034)	0.338 (0.081)	0.002804 (0.000513)	0.485 (0.016)	0.317 (0.017)	0.001024 (0.001517)
	BDETT	0.243 (**0.006**)	0.184 (**0.006**)	0.001306 (**0.000154**)	0.217 (**0.005**)	0.154 (**0.006**)	0.001058 (**0.000106**)

Assessment—Ablation Studies

The ablation study results are reported in the rows named "DET only" and "DTT only" in Tables 7, 8, and 9. In addition, the results are illustrated in Figure 5. The results reflect the same facts that we observed in the obstacle avoidance tasks. The dynamic threshold schemes with only the DET or DTT components cannot effectively regulate the firing rate statuses of the host SNNs, prohibiting meaningful homeostasis. For the LIF-based host SNNs, one extreme example is illustrated in the "30% Zero weight" sections of Figures 5c and e, where 'DTT only' reports the largest change among all competing approaches under all experimental conditions in terms of ΔFR_{std}^m. With the $T = 25$ setup, as shown in Figures 5d and f, the ΔFR_m values of 'DTT only' in the "GN weight" sections are the largest across all experimental settings.

16

Table 11: The raw homeostasis measurements and the corresponding changes with respect to the baseline condition in Mujoco HalfCheetah-v3 tasks with the $T = 25$ setup.

Type	Name	LIF ($T = 25$)			SRM ($T = 25$)		
		$\text{FR}_m(\Delta)$	$\text{FR}_{std}^m(\Delta)$	$\text{FR}_{std}^s(\Delta)$	$\text{FR}_m(\Delta)$	$\text{FR}_{std}^m(\Delta)$	$\text{FR}_{std}^s(\Delta)$
baseline condition	PopSAN	0.436	0.230	0.001156	0.440	0.252	0.002217
	DT1 [4]	0.420	0.240	0.001158	0.470	0.247	0.001869
	DT2 [5]	0.676	0.290	0.000939	0.521	0.305	0.001785
	DET only	0.292	0.225	0.001237	0.341	0.253	0.001631
	DTT only	0.635	0.257	0.002433	0.493	0.340	0.002722
	BDETT	0.251	0.192	0.001292	0.215	0.173	0.001074
Random joint position	PopSAN	0.426 (0.010)	0.238 (0.008)	0.001381 (0.000225)	0.458 (0.018)	0.264 (0.012)	0.003048 (0.000831)
	DT1 [4]	0.440 (0.020)	0.258 (0.018)	0.001721 (0.000563)	0.442 (0.028)	0.268 (0.021)	0.003632 (0.001763)
	DT2 [5]	0.648 (0.028)	0.272 (0.018)	0.001348 (0.000409)	0.501 (0.020)	0.342 (0.037)	0.002384 (0.000599)
	DET only	0.301 (0.009)	0.236 (0.011)	0.001464 (0.000227)	0.359 (0.018)	0.285 (0.032)	0.002179 (0.000548)
	DTT only	0.630 (0.005)	0.265 (0.008)	0.002104 (0.000329)	0.518 (0.025)	0.372 (0.032)	0.003438 (0.000716)
	BDETT	0.247 (**0.004**)	0.187 (**0.005**)	0.001431 (**0.000139**)	0.210 (**0.005**)	0.163 (**0.010**)	0.001242 (**0.000168**)
Random joint velocity	PopSAN	0.450 (0.014)	0.239 (0.009)	0.001425 (0.000269)	0.474 (0.034)	0.332 (0.080)	0.002922 (0.000705)
	DT1 [4]	0.387 (0.033)	0.258 (0.018)	0.002474 (0.001316)	0.427 (0.043)	0.268 (0.021)	0.003572 (0.001703)
	DT2 [5]	0.664 (0.012)	0.261 (0.029)	0.002582 (0.001643)	0.487 (0.034)	0.347 (0.042)	0.002529 (0.000744)
	DET only	0.310 (0.018)	0.235 (0.010)	0.001582 (0.000345)	0.368 (0.027)	0.292 (0.039)	0.002544 (0.000913)
	DTT only	0.627 (0.008)	0.269 (0.012)	0.001548 (0.000885)	0.515 (0.022)	0.370 (0.030)	0.003282 (0.000560)
	BDETT	0.245 (**0.006**)	0.185 (**0.007**)	0.001478 (**0.000186**)	0.208 (**0.007**)	0.183 (**0.010**)	0.001305 (**0.000231**)
GN	PopSAN	0.423 (0.013)	0.252 (0.022)	0.001633 (0.000477)	0.403 (0.037)	0.236 (0.016)	0.002574 (0.000357)
	DT1 [4]	0.433 (0.013)	0.221 (0.019)	0.002061 (0.000903)	0.552 (0.082)	0.271 (0.024)	0.003784 (0.001915)
	DT2 [5]	0.642 (0.034)	0.310 (0.020)	0.001385 (0.000446)	0.480 (0.041)	0.373 (0.068)	0.002833 (0.001048)
	DET only	0.281 (0.011)	0.219 (**0.006**)	0.001610 (0.000373)	0.304 (0.037)	0.290 (0.037)	0.003082 (0.001451)
	DTT only	0.622 (0.013)	0.274 (0.017)	0.002762 (0.000329)	0.453 (0.040)	0.305 (0.035)	0.002048 (0.000674)
	BDETT	0.243 (**0.008**)	0.184 (0.008)	0.001512 (**0.000220**)	0.226 (**0.011**)	0.180 (**0.007**)	0.001283 (**0.000209**)
8-bit Loihi weight	PopSAN	0.432 (0.004)	0.224 (0.006)	0.001310 (0.000154)	0.452 (0.012)	0.238 (0.014)	0.001849 (0.000368)
	DT1 [4]	0.427 (0.007)	0.221 (0.019)	0.001035 (0.000123)	0.485 (0.015)	0.259 (0.012)	0.002363 (0.000494)
	DT2 [5]	0.661 (0.006)	0.278 (0.012)	0.001174 (0.000235)	0.535 (0.014)	0.328 (0.023)	0.001976 (0.000191)
	DET only	0.299 (0.007)	0.234 (0.009)	0.001379 (0.000142)	0.351 (0.010)	0.267 (0.014)	0.001275 (0.000356)
	DTT only	0.644 (0.009)	0.242 (0.015)	0.002210 (0.000223)	0.506 (0.013)	0.354 (0.014)	0.002894 (0.000172)
	BDETT	0.250 (**0.001**)	0.197 (**0.005**)	0.001393 (**0.000101**)	0.211 (**0.004**)	0.178 (**0.005**)	0.001169 (**0.000094**)
GN weight	PopSAN	0.471 (0.035)	0.211 (0.019)	0.001637 (0.000481)	0.479 (0.039)	0.336 (0.084)	0.003181 (0.000964)
	DT1 [4]	0.433 (**0.013**)	0.218 (0.022)	0.000904 (0.000254)	0.438 (0.032)	0.302 (0.055)	0.004041 (0.002172)
	DT2 [5]	0.642 (0.034)	0.320 (0.030)	0.001683 (0.000744)	0.492 (0.029)	0.366 (0.061)	0.004585 (0.002800)
	DET only	0.271 (0.021)	0.238 (0.013)	0.001720 (0.000483)	0.369 (0.028)	0.202 (0.051)	0.003927 (0.002296)
	DTT only	0.607 (0.028)	0.289 (0.032)	0.003104 (0.000671)	0.569 (0.076)	0.301 (0.039)	0.004273 (0.001551)
	BDETT	0.264 (**0.013**)	0.183 (**0.009**)	0.001512 (**0.000220**)	0.229 (**0.014**)	0.182 (**0.009**)	0.001199 (**0.000125**)
30% Zero weight	PopSAN	0.493 (0.057)	0.215 (0.015)	0.001892 (0.000736)	0.410 (0.030)	0.292 (0.040)	0.003237 (0.001020)
	DT1 [4]	0.447 (0.027)	0.258 (0.018)	0.001859 (0.000701)	0.424 (0.046)	0.288 (0.041)	0.000926 (0.000943)
	DT2 [5]	0.655 (0.021)	0.334 (0.044)	0.001674 (0.000735)	0.486 (0.035)	0.251 (0.054)	0.000896 (0.000889)
	DET only	0.273 (0.019)	0.239 (0.014)	0.001692 (0.000455)	0.371 (0.030)	0.216 (0.037)	0.004106 (0.002475)
	DTT only	0.677 (0.042)	0.305 (0.048)	0.002976 (0.000543)	0.426 (0.067)	0.312 (0.028)	0.001176 (0.001546)
	BDETT	0.239 (**0.012**)	0.181 (**0.011**)	0.001642 (**0.000350**)	0.221 (**0.006**)	0.180 (**0.007**)	0.001183 (**0.000109**)

17

Supplementary Note 6: Additional Details on Continuous Control Experiments—Ant-v3

The training and experimental setups are the same as those used for the HalfCheetah-v3 tasks.
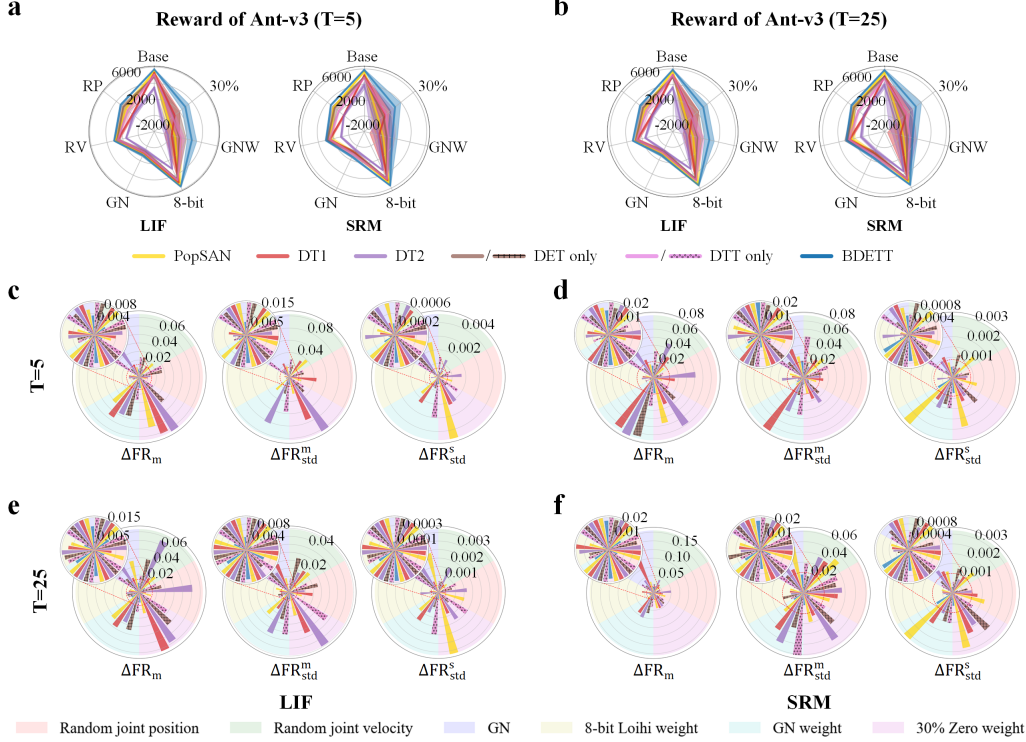
Figure 6: The experimental results obtained in the Ant-v3 tasks. a & b. The rewards obtained under normal and different degraded conditions under the $T = 5$ and $T = 25$ settings, respectively. 'Base' denotes the base condition; 'RP' and 'RV' represent random joint position and random joint velocity, respectively; '8-bit', 'GNW', and '30%' denote the 8-bit Loihi weights, GN weights, and 30% zero weights, respectively. c & d. Homeostasis measurements obtained under the $T = 5$ setting for the LIF- and SRM-based host SNNs, respectively. e & f. Homeostasis results obtained with the $T = 25$ setup for the LIF- and SRM-based host SNNs, respectively.

Assessment—Reward

As in the HalfCheetah-v3 tasks, we present the rewards of all competing host SNNs under the original normal conditions with the $T = 5$ and $T = 25$ settings; see Table 12. Compared to HalfCheetah-v3's 17-dimensional state, the state of an Ant-v3 task has 111 dimensions. Thus, the rewards obtained from the Ant-v3 experiments are much lower than those obtained in the HalfCheetah-v3 tasks. Nevertheless, the proposed BDETT offers the highest rewards in the Ant-v3 tasks, and it improves upon the rewards of the LIF- and SRM-based baseline models by at least 173 and 236, respectively.

Relative to the HalfCheetah-v3 tasks, DT1 offers much better rewards in the Ant-v3 tasks under normal conditions. However, the rewards provided by DT1 and DT2 are still lower than those of the baseline PopSAN model. This observation is consistent with those obtained in the obstacle avoidance and HalfCheetah-v3 experiments.

We show the quantitative performance of all competing methods under degraded input and weight uncertainty conditions in Tables 13 and 14, respectively. In Figures 6a and b, we also intuitively present the results. The proposed BDETT is still the best performer under all experimental conditions based on the obtained results. A more detailed analysis for each degraded condition is provided in the following.

18

Table 12: Quantitative performance of Mujoco Ant-v3 tasks under standard testing condition.

Name	LIF ($T = 5$) Reward↑	SRM ($T = 5$) Reward↑	LIF ($T = 25$) Reward↑	SRM ($T = 25$) Reward↑
PopSAN	5526 (σ-81)	5643 (σ-84)	5711 (σ-105)	5612 (σ-105)
DT1 [4]	5272 (σ-142)	5179 (σ-157)	5218 (σ-164)	5121 (σ-117)
DT2 [5]	3454 (σ-183)	3925 (σ-483)	3628 (σ-180)	4016 (σ-445)
DET only	4836 (σ-82)	4971 (σ-128)	4957 (σ-113)	5125 (σ-144)
DTT only	5041 (σ-294)	4883 (σ-154)	5192 (σ-267)	4864 (σ-187)
BDETT	**5726** (σ-61)	**5879** (σ-117)	**5884** (σ-97)	**5942** (σ-136)

Table 13: Quantitative performance of Mujoco Ant-v3 tasks under degraded input conditions.

Type	Name	LIF ($T = 5$) Reward↑	SRM ($T = 5$) Reward↑	LIF ($T = 25$) Reward↑	SRM ($T = 25$) Reward↑
	PopSAN	2503 (σ-503)	3004 (σ-131)	2544 (σ-337)	3036 (σ-152)
	DT1 [4]	1435 (σ-130)	1333 (σ-122)	1380 (σ-158)	1258 (σ-150)
Random	DT2 [5]	1280 (σ-234)	1330 (σ-99)	1335 (σ-206)	1364 (σ-152)
joint	DET only	2907 (σ-320)	2836 (σ-392)	2862 (σ-342)	2994 (σ-332)
position	DTT only	2213 (σ-389)	2190 (σ-119)	2305 (σ-373)	2273 (σ-162)
	BDETT	**3339** (σ-111)	**3450** (σ-75)	**3320** (σ-126)	**3427** (σ-115)
	PopSAN	2890 (σ-115)	2372 (σ-390)	2858 (σ-149)	2287 (σ-427)
Random	DT1 [4]	2628 (σ-232)	2508 (σ-166)	2643 (σ-259)	2574 (σ-232)
joint	DT2 [5]	1579 (σ-89)	1025 (σ-139)	1595 (σ-131)	1009 (σ-208)
velocity	DET only	2720 (σ-365)	2809 (σ-296)	2802 (σ-197)	2896 (σ-372)
	DTT only	2635 (σ-234)	2515 (σ-201)	2699 (σ-255)	2618 (σ-260)
	BDETT	**3103** (σ-95)	**2984** (σ-176)	**3217** (σ-119)	**2996** (σ-195)
	PopSAN	977 (σ-320)	1031 (σ-212)	1022 (σ-358)	1059 (σ-217)
	DT1 [4]	922 (σ-234)	958 (σ-156)	875 (σ-270)	1012 (σ-178)
GN	DT2 [5]	560 (σ-179)	583 (σ-158)	664 (σ-163)	623 (σ-235)
	DET only	782 (σ-246)	1048 (σ-345)	844 (σ-304)	1105 (σ-364)
	DTT only	849 (σ-177)	1172 (σ-209)	906 (σ-170)	1255 (σ-218)
	BDETT	**1269** (σ-166)	**1559** (σ-138)	**1339** (σ-156)	**1576** (σ-161)

Degraded Inputs Compared to that of a HalfCheetah-v3 agent, the observation (state) of an Ant-v3 agent s represents a 111-dimensional data consisting of 13-dimensional joint position information, 14-dimensional joint velocity information, and 84-dimensional contact force data. We disturb Ant-v3's observation in the same three ways introduced in the HalfCheetah-v3 tasks: "Random joint position", "Random joint velocity", and "GN". The average rewards obtained in the ten evaluations conducted under these three different conditions are shown in Table 13. Under all experimental settings, the proposed BDETT offers the host SNNs the highest rewards, significantly improving upon the reward of the baseline PopSAN model by at least 213.

Weight Uncertainty We leverage the same weight uncertainty conditions as those used in the robot obstacle avoidance and HalfCheetah-v3 experiments. The experimental results are shown in Table 14. The proposed BDETT remains the best performer under all weight uncertainty conditions. As in the HalfCheetah-v3 experiments, even with low-precision 8-bit weights, the proposed BDETT helps both the LIF- and SRM-based host SNNs achieve higher rewards than those offered by the baseline counterparts with high-precision floating-point weights under $T = 5$ (5570 vs. 5526 and 5648 vs. 5643, respectively). With the $T = 25$ setup, the SRM-based host SNN exhibits the same pattern.

Assessment—Homeostatic

The raw homeostasis measurements obtained with both T=5 and T=25 are provided in Tables 15 and 16, respectively. The corresponding homeostasis plots are shown in Figures 6c-f.

The homeostasis results obtained in the Ant-v3 tasks demonstrate the effectiveness of the proposed BDETT in terms of regulating the neuronal firing rates of the host SNNs, inducing minimal changes in all three metrics when transferring from the base conditions to all other experimental settings. We witness that the strongest homeostasis again provides the highest rewards.

19

Table 14: Quantitative performance of Mujoco Ant-v3 tasks with weight uncertainty conditions.

Type	Name	LIF ($T=5$) Reward↑	SRM ($T=5$) Reward↑	LIF ($T=25$) Reward↑	SRM ($T=25$) Reward↑
8-bit Loihi weight	PopSAN	5347 (σ-175)	5285 (σ-158)	5504 (σ-210)	5228 (σ-139)
	DT1 [4]	5004 (σ-88)	4889 (σ-163)	4826 (σ-102)	4902 (σ-182)
	DT2 [5]	3122 (σ-77)	3463 (σ-99)	3266 (σ-93)	3676 (σ-86)
	DET only	4561 (σ-135)	4634 (σ-111)	4663 (σ-156)	4727 (σ-153)
	DTT only	4703 (σ-56)	4722 (σ-87)	4903 (σ-63)	4779 (σ-126)
	BDETT	**5570** (σ-59)	**5648** (σ-73)	**5606** (σ-52)	**5620** (σ-143)
GN weight	PopSAN	637 (σ-860)	467 (σ-951)	667 (σ-1002)	444 (σ-1105)
	DT1 [4]	221 (σ-949)	-57 (σ-1245)	155 (σ-839)	6 (σ-1722)
	DT2 [5]	-265 (σ-488)	-173 (σ-640)	-226 (σ-628)	-198 (σ-883)
	DET only	1208 (σ-855)	940 (σ-750)	1258 (σ-638)	923 (σ-883)
	DTT only	1392 (σ-467)	1204 (σ-746)	1448 (σ-644)	1310 (σ-867)
	BDETT	**2782** (σ-599)	**1658** (σ-640)	**2780** (σ-621)	**1669** (σ-612)
30% Zero weight	PopSAN	287 (σ-524)	372 (σ-994)	273 (σ-633)	407 (σ-959)
	DT1 [4]	1247 (σ-801)	1450 (σ-863)	1200 (σ-1020)	1552 (σ-996)
	DT2 [5]	-548 (σ-354)	-203 (σ-901)	-563 (σ-743)	-183 (σ-1125)
	DET only	1007 (σ-960)	1136 (σ-1179)	1084 (σ-1092)	1186 (σ-1084)
	DTT only	908 (σ-428)	1559 (σ-1167)	1038 (σ-487)	1563 (σ-1049)
	BDETT	**2931** (σ-544)	**3046** (σ-886)	**2978** (σ-605)	**3152** (σ-924)

Table 15: The raw homeostasis measurements and the corresponding changes with respect to the baseline condition in Mujoco Ant-v3 tasks with the $T=5$ setting.

Type	Name	LIF ($T=5$) $FR_m(\Delta)$	$FR_{std}^m(\Delta)$	$FR_{std}^s(\Delta)$	SRM ($T=5$) $FR_m(\Delta)$	$FR_{std}^m(\Delta)$	$FR_{std}^s(\Delta)$
baseline condition	PopSAN	0.548	0.262	0.002169	0.197	0.150	0.001823
	DT1 [4]	0.531	0.253	0.002483	0.446	0.251	0.002172
	DT2 [5]	0.770	0.223	0.004427	0.580	0.167	0.003238
	DET only	0.289	0.246	0.001820	0.328	0.187	0.002027
	DTT only	0.547	0.280	0.001554	0.443	0.276	0.002942
	BDETT	0.271	0.204	0.001325	0.213	0.199	0.001535
Random joint position	PopSAN	0.556 (0.008)	0.242 (0.020)	0.003210 (0.001041)	0.208 (0.011)	0.134 (0.016)	0.003022 (0.001199)
	DT1 [4]	0.521 (0.010)	0.209 (0.044)	0.002859 (0.000376)	0.420 (0.026)	0.275 (0.024)	0.002819 (0.000647)
	DT2 [5]	0.757 (0.013)	0.211 (0.012)	0.002735 (0.001692)	0.529 (0.051)	0.188 (0.021)	0.002521 (0.000717)
	DET only	0.262 (0.027)	0.270 (0.024)	0.002575 (0.000755)	0.339 (0.011)	0.210 (0.023)	0.002831 (0.000804)
	DTT only	0.519 (0.028)	0.256 (0.024)	0.002481 (0.000927)	0.430 (0.013)	0.244 (0.032)	0.002454 (0.000488)
	BDETT	0.275 (**0.004**)	0.209 (**0.005**)	0.001240 (**0.000085**)	0.207 (**0.006**)	0.192 (**0.007**)	0.001308 (**0.000227**)
Random joint velocity	PopSAN	0.526 (0.022)	0.223 (0.039)	0.001743 (0.000426)	0.180 (0.017)	0.117 (0.033)	0.003239 (0.001416)
	DT1 [4]	0.516 (0.015)	0.221 (0.032)	0.003031 (0.000548)	0.415 (0.031)	0.278 (0.027)	0.002766 (0.000594)
	DT2 [5]	0.760 (0.010)	0.220 (0.003)	0.003049 (0.001378)	0.534 (0.046)	0.182 (0.015)	0.002749 (0.000489)
	DET only	0.265 (0.024)	0.266 (0.020)	0.001443 (0.000377)	0.345 (0.014)	0.206 (0.019)	0.003182 (0.001155)
	DTT only	0.524 (0.023)	0.251 (0.029)	0.003020 (0.001466)	0.410 (0.033)	0.225 (0.051)	0.002385 (0.000557)
	BDETT	0.265 (**0.006**)	0.206 (**0.002**)	0.001452 (**0.000127**)	0.207 (**0.006**)	0.193 (**0.006**)	0.001882 (**0.000347**)
GN	PopSAN	0.560 (0.012)	0.244 (0.018)	0.004782 (0.002613)	0.180 (0.017)	0.123 (0.027)	0.002589 (0.000766)
	DT1 [4]	0.515 (0.016)	0.229 (0.024)	0.002723 (0.000240)	0.470 (0.024)	0.289 (0.038)	0.003259 (0.001087)
	DT2 [5]	0.727 (0.043)	0.238 (0.015)	0.002130 (0.002297)	0.527 (0.053)	0.204 (0.037)	0.004192 (0.000954)
	DET only	0.302 (0.013)	0.260 (0.014)	0.003762 (0.001942)	0.312 (0.016)	0.161 (0.026)	0.002495 (**0.000468**)
	DTT only	0.506 (0.041)	0.241 (0.039)	0.003306 (0.001752)	0.390 (0.053)	0.320 (0.044)	0.004334 (0.001392)
	BDETT	0.262 (**0.009**)	0.198 (**0.006**)	0.001539 (**0.000214**)	0.198 (**0.015**)	0.178 (**0.021**)	0.002068 (0.000533)
8-bit Loihi weight	PopSAN	0.540 (0.008)	0.269 (0.007)	0.001838 (0.000331)	0.206 (0.009)	0.167 (0.017)	0.001602 (0.000221)
	DT1 [4]	0.519 (0.012)	0.261 (0.008)	0.002217 (0.000266)	0.459 (0.013)	0.237 (0.014)	0.002406 (0.000234)
	DT2 [5]	0.758 (0.012)	0.217 (0.006)	0.003884 (0.000543)	0.566 (0.014)	0.193 (0.026)	0.002513 (0.000725)
	DET only	0.281 (0.008)	0.250 (0.004)	0.001933 (0.000113)	0.323 (0.005)	0.194 (0.007)	0.001869 (0.000158)
	DTT only	0.539 (0.008)	0.286 (0.006)	0.001463 (0.000091)	0.433 (0.010)	0.285 (0.009)	0.003206 (0.000264)
	BDETT	0.274 (**0.003**)	0.206 (**0.002**)	0.001280 (**0.000045**)	0.215 (**0.002**)	0.203 (**0.004**)	0.001602 (**0.000067**)
GN weight	PopSAN	0.507 (0.041)	0.291 (0.029)	0.003844 (0.001675)	0.190 (0.007)	0.138 (0.012)	0.004859 (0.003036)
	DT1 [4]	0.475 (0.056)	0.261 (0.008)	0.004749 (0.002266)	0.519 (0.073)	0.328 (0.077)	0.003441 (0.001269)
	DT2 [5]	0.722 (0.048)	0.305 (0.082)	0.003632 (0.000795)	0.503 (0.077)	0.212 (0.045)	0.004833 (0.001595)
	DET only	0.242 (0.047)	0.218 (0.028)	0.000966 (0.000854)	0.402 (0.074)	0.209 (0.022)	0.003346 (0.001319)
	DTT only	0.520 (0.027)	0.223 (0.057)	0.004540 (0.002986)	0.408 (0.035)	0.322 (0.046)	0.004416 (0.001474)
	BDETT	0.268 (**0.003**)	0.208 (**0.004**)	0.001548 (**0.000223**)	0.208 (**0.005**)	0.190 (**0.009**)	0.002351 (**0.000816**)
30% Zero weight	PopSAN	0.488 (0.060)	0.290 (0.028)	0.006801 (0.004632)	0.140 (0.057)	0.130 (0.020)	0.004246 (0.002423)
	DT1 [4]	0.460 (0.071)	0.328 (0.075)	0.004668 (0.002185)	0.411 (0.035)	0.223 (0.028)	0.003402 (0.001230)
	DT2 [5]	0.696 (0.074)	0.326 (0.103)	0.002308 (0.002119)	0.511 (0.069)	0.203 (0.036)	0.004283 (0.001045)
	DET only	0.250 (0.039)	0.279 (0.033)	0.001023 (0.000797)	0.364 (0.036)	0.213 (0.026)	0.003631 (0.001604)
	DTT only	0.566 (0.019)	0.308 (0.028)	0.003243 (0.001689)	0.465 (0.022)	0.268 (**0.008**)	0.003563 (**0.000621**)
	BDETT	0.258 (**0.013**)	0.217 (**0.013**)	0.001840 (**0.000515**)	0.194 (**0.019**)	0.191 (**0.008**)	0.002276 (0.000741)

20

Table 16: The raw homeostasis measurements and the corresponding changes with respect to the baseline condition in Mujoco Ant-v3 tasks with the $T = 25$ setup.

Type	Name	LIF ($T=25$)			SRM ($T=25$)		
		$\text{FR}_m(\Delta)$	$\text{FR}^m_{std}(\Delta)$	$\text{FR}^s_{std}(\Delta)$	$\text{FR}_m(\Delta)$	$\text{FR}^m_{std}(\Delta)$	$\text{FR}^s_{std}(\Delta)$
baseline condition	PopSAN	0.535	0.258	0.002247	0.213	0.166	0.002027
	DT1 [4]	0.530	0.252	0.002688	0.453	0.244	0.001694
	DT2 [5]	0.753	0.230	0.004728	0.563	0.182	0.003493
	DET only	0.302	0.250	0.001947	0.334	0.192	0.001872
	DTT only	0.541	0.276	0.001526	0.451	0.281	0.002485
	BDETT	0.275	0.204	0.001503	0.222	0.195	0.001829
Random joint position	PopSAN	0.549 (0.014)	0.242 (0.016)	0.003794 (0.001547)	0.248 (0.035)	0.140 (0.026)	0.003682 (0.001655)
	DT1 [4]	0.522 (0.008)	0.223 (0.029)	0.003074 (0.000386)	0.426 (0.027)	0.277 (0.033)	0.002951 (0.001257)
	DT2 [5]	0.692 (0.061)	0.211 (0.019)	0.003076 (0.001652)	0.513 (0.050)	0.219 (0.037)	0.002523 (0.000970)
	DET only	0.276 (0.026)	0.286 (0.036)	0.002744 (0.000797)	0.352 (0.018)	0.224 (0.032)	0.002642 (0.000770)
	DTT only	0.520 (0.021)	0.252 (0.024)	0.002636 (0.001110)	0.430 (0.021)	0.246 (0.035)	0.002206 (0.000279)
	BDETT	0.280 (**0.005**)	0.210 (**0.006**)	0.001386 (**0.000117**)	0.216 (**0.006**)	0.188 (**0.007**)	0.001682 (**0.000147**)
Random joint velocity	PopSAN	0.510 (0.025)	0.224 (0.034)	0.001589 (0.000658)	0.189 (0.024)	0.121 (0.045)	0.003472 (0.001445)
	DT1 [4]	0.510 (0.020)	0.220 (0.032)	0.003236 (0.000548)	0.424 (0.029)	0.281 (0.037)	0.002692 (0.000998)
	DT2 [5]	0.688 (0.065)	0.203 (0.027)	0.003163 (0.001565)	0.522 (0.041)	0.220 (0.038)	0.002732 (0.000761)
	DET only	0.263 (0.039)	0.294 (0.044)	0.002583 (0.000636)	0.353 (0.019)	0.209 (0.017)	0.003135 (0.001263)
	DTT only	0.522 (0.019)	0.259 (0.017)	0.002184 (0.000658)	0.426 (0.025)	0.252 (0.029)	0.001921 (0.000564)
	BDETT	0.267 (**0.008**)	0.206 (**0.002**)	0.001632 (**0.000129**)	0.213 (**0.009**)	0.190 (**0.005**)	0.002005 (**0.000176**)
GN	PopSAN	0.572 (0.037)	0.240 (0.018)	0.004581 (0.002334)	0.180 (0.033)	0.120 (0.046)	0.003148 (0.001121)
	DT1 [4]	0.512 (0.018)	0.214 (0.038)	0.002012 (0.000676)	0.633 (**0.018**)	0.269 (0.025)	0.002885 (0.001191)
	DT2 [5]	0.718 (0.035)	0.259 (0.029)	0.002833 (0.001895)	0.520 (0.043)	0.232 (0.050)	0.002148 (0.001345)
	DET only	0.323 (0.021)	0.299 (0.049)	0.003665 (0.001718)	0.305 (0.029)	0.169 (0.023)	0.002684 (0.000812)
	DTT only	0.512 (0.029)	0.244 (0.032)	0.003522 (0.001996)	0.412 (0.039)	0.328 (0.047)	0.003144 (0.000659)
	BDETT	0.264 (**0.011**)	0.200 (**0.004**)	0.001400 (**0.000103**)	0.204 (0.018)	0.177 (**0.018**)	0.002129 (**0.000300**)
8-bit Loihi weight	PopSAN	0.546 (0.011)	0.275 (0.017)	0.002569 (0.000322)	0.225 (0.012)	0.179 (0.013)	0.002581 (0.000554)
	DT1 [4]	0.542 (0.012)	0.264 (0.012)	0.003189 (0.000501)	0.421 (0.032)	0.257 (0.013)	0.001184 (0.000510)
	DT2 [5]	0.738 (0.015)	0.220 (0.010)	0.003680 (0.001048)	0.545 (0.018)	0.194 (0.012)	0.003026 (0.000467)
	DET only	0.316 (0.014)	0.236 (0.014)	0.002292 (0.000345)	0.346 (0.012)	0.212 (0.020)	0.002214 (0.000342)
	DTT only	0.554 (0.013)	0.290 (0.014)	0.001174 (0.000352)	0.438 (0.013)	0.294 (0.013)	0.002763 (0.000278)
	BDETT	0.270 (**0.005**)	0.200 (**0.004**)	0.001576 (**0.000073**)	0.218 (**0.004**)	0.199 (**0.004**)	0.001722 (**0.000107**)
GN weight	PopSAN	0.493 (0.042)	0.295 (0.037)	0.003726 (0.001479)	0.190 (0.023)	0.141 (0.025)	0.005216 (0.003189)
	DT1 [4]	0.482 (0.048)	0.277 (0.025)	0.004663 (0.001975)	0.522 (0.069)	0.287 (0.043)	0.003540 (0.001846)
	DT2 [5]	0.715 (0.038)	0.286 (0.056)	0.003431 (0.001297)	0.486 (0.077)	0.235 (0.053)	0.004632 (0.001139)
	DET only	0.257 (0.045)	0.215 (0.035)	0.001036 (0.000911)	0.394 (0.060)	0.227 (0.035)	0.003373 (0.001501)
	DTT only	0.518 (0.023)	0.223 (0.053)	0.003998 (0.002472)	0.410 (0.041)	0.342 (0.061)	0.004025 (0.001540)
	BDETT	0.265 (**0.010**)	0.211 (**0.007**)	0.001729 (**0.000226**)	0.212 (**0.010**)	0.206 (**0.011**)	0.002773 (**0.000944**)
30% Zero weight	PopSAN	0.510 (0.025)	0.288 (0.030)	0.005942 (0.003695)	0.168 (0.045)	0.137 (0.029)	0.004893 (0.002866)
	DT1 [4]	0.457 (0.073)	0.307 (0.055)	0.004043 (0.001355)	0.406 (0.047)	0.220 (0.024)	0.003909 (0.002215)
	DT2 [5]	0.685 (0.068)	0.309 (0.079)	0.002863 (0.001865)	0.517 (0.046)	0.236 (0.054)	0.005426 (0.001933)
	DET only	0.252 (0.050)	0.243 (**0.007**)	0.001132 (0.000815)	0.376 (0.042)	0.232 (0.040)	0.004387 (0.002515)
	DTT only	0.579 (0.038)	0.332 (0.056)	0.003538 (0.002012)	0.487 (0.036)	0.256 (0.025)	0.003692 (0.001207)
	BDETT	0.263 (**0.012**)	0.213 (0.009)	0.001883 (**0.000380**)	0.204 (**0.018**)	0.183 (**0.012**)	0.002485 (**0.000656**)

Assessment—Ablation Studies

The experimental results obtained in the Ant-v3 task ablation studies under different conditions are reported in the rows named 'DET only' and 'DTT only' in Tables 12, 13, and 14. All listed evaluations validate that the BDETT scheme performs better than any single component. As shown in Table 14, under the "GN weight" condition, both 'DET only' and 'DTT only' offer both the LIF- and SRM-based host SNNs higher rewards than the other competing dynamic threshold schemes. As in the other tasks, the dynamic threshold scheme with only one component cannot effectively regulate the firing rate statuses of the host SNNs, prohibiting meaningful homeostasis. When combining the DTT and DET components, we witness much more stable homeostasis for all host SNNs.

21

Table 17: Quantitative performance of obstacle avoidance tasks with different constant coefficient settings under static obstacle condition.

Constant	LIF ($T = 5$) SR↑	SRM ($T = 5$) SR↑
0.1	97.5%	**96.5%**
0.2(original)	**98.5%**	**96.5%**
0.3	**98.5%**	**96.5%**
0.4	97.5%	95.5%
0.5	98%	95%
1.0	93.5%	91.5%

Table 18: Quantitative performance of obstacle avoidance tasks with different constant coefficient settings under dynamic obstacle condition.

Constant	LIF ($T = 5$) SR↑	SRM ($T = 5$) SR↑
0.1	91.5%	**90.5%**
0.2(original)	**92.5%**	**90.5%**
0.3	92%	90%
0.4	92%	89%
0.5	91%	89%
1.0	86%	80.5%

Supplementary Note 7: Impact of Constant Coefficient '0.2' in the DET

In the proposed DET component, a constant '0.2' is used for balancing the contributions of the specifically designed bias items, $0.2(\max(v_i^l(t)) - \min(v_i^l(t)))$ and $0.2(\max(\Theta_i^l(t)) - \min(\Theta_i^l(t)))$.

Based on our experimental results, the effectiveness of the proposed BDETT is not sensitive to this value. In the obstacle avoidance tasks (see Tables 18, 19, and 20), when the constant value is within the range of $[0.1, 0.5]$, the standard deviations of the SRs for the LIF- and SRM-based host SNNs are 0.005 and 0.007, respectively. More importantly, even with an extreme value of 1.0, the corresponding SRs are higher than those offered by all other competing dynamic threshold approaches.

In the HalfCheetah-v3 tasks (see Tables 21, 22, and 23) and the Ant-v3 tasks (see Table 24, 25, and 26), the proposed BDETT method is more sensitive to the coefficient value than in the obstacle avoidance tasks. When the constant value is within the range of $[0.1, 0.5]$, the standard deviations of the rewards are 94 and 107 for the LIF- and SRM-based host SNNs in the HalfCheetah-v3 tasks, respectively. In the Ant-v3 experiments, the LIF- and SRM-based SNNs provide rewards of 114 and 111, respectively. With the extreme value of 1.0, under some experimental conditions, the rewards offered by our approach are still higher than those provided by other methods (e.g., the "30% zero weight" condition of HalfCheetah-v3 and the "GN weight" condition of Ant-v3). However, with the extreme value of 1.0, the effectiveness of the proposed BDETT scheme is reduced. This means that the sensitivity to the constant value increases as the complexity of the given task increases.

Note that the value of '0.2' offers the most effective and robust performance across all three tasks under all experimental conditions. Therefore, we set the coefficient to '0.2' in our proposed dynamic threshold scheme.

Table 19: Quantitative performance of obstacle avoidance tasks with different constant coefficient settings under degraded input conditions.

Type	Constant	LIF ($T = 5$) SR↑	SRM ($T = 5$) SR↑	Type	Constant	LIF ($T = 5$) SR↑	SRM ($T = 5$) SR↑	Type	Constant	LIF ($T = 5$) SR↑	SRM ($T = 5$) SR↑
	0.1	89%	78%		0.1	83.5%	82%		0.1	83.5%	82%
	0.2(original)	**90%**	**79.5%**		0.2(original)	**84.5%**	**83%**		0.2(original)	**84.5%**	**82.5%**
	0.3	89%	77.5%		0.3	83%	81.5%		0.3	84%	82%
0.2	0.4	87%	75%	0.6	0.4	82%	79%	GN	0.4	84%	81.5%
	0.5	87.5%	75%		0.5	81.5%	80.5%		0.5	83%	81%
	1.0	83.5%	70.5%		1.0	76%	76.5%		1.0	77%	70.5%

22

Table 20: Quantitative performance of obstacle avoidance tasks with different constant coefficient settings under weight uncertainty conditions.

Type	Constant	LIF ($T=5$) SR↑	SRM ($T=5$) SR↑	Type	Constant	LIF ($T=5$) SR↑	SRM ($T=5$) SR↑	Type	Constant	LIF ($T=5$) SR↑	SRM ($T=5$) SR↑
	0.1	89.5%	87.5%		0.1	87.2%	60.5%		0.1	**77.2%**	64.0%
8-bit	0.2(original)	**90%**	**88.5%**	GN	0.2(original)	**87.7%**	**61.8%**	30%	0.2(original)	**77.2%**	**65.2%**
Loihi	0.3	**90%**	88%	weight	0.3	86.3%	60.0%	Zero	0.3	75.8%	64.2%
weight	0.4	88.5%	88%	(5 rounds)	0.4	85.7%	58.6%	weight	0.4	74.3%	63.5%
	0.5	87.5%	87%		0.5	84.1%	57.4%	(5 rounds)	0.5	72.8%	83.6%
	1.0	83%	79.5%		1.0	80.3%	52.3%		1.0	67.1%	52.9%

Table 21: Quantitative performance of HalfCheetah-v3 tasks with different constant coefficient settings under standard testing conditions.

Constant	LIF ($T=5$) Reward↑	SRM ($T=5$) Reward↑
0.1	11029	11903
0.2(original)	**11064**	**11960**
0.3	10987	11875
0.4	10976	11682
0.5	10793	11724
1.0	10028	11123

Table 22: Quantitative performance of HalfCheetah-v3 tasks with different constant coefficient settings under degraded input conditions.

Type	Constant	LIF ($T=5$) Reward↑	SRM ($T=5$) Reward↑	Type	Constant	LIF ($T=5$) Reward↑	SRM ($T=5$) Reward↑	Type	Constant	LIF ($T=5$) Reward↑	SRM ($T=5$) Reward↑
	0.1	8379	7767		0.1	8241	7023		0.1	3832	3825
	0.2(original)	**8465**	**7883**	Random	0.2(original)	**8302**	**7116**		0.2(original)	**3909**	**3895**
Random	0.3	8302	7748	joint	0.3	8159	6968	GN	0.3	3790	3810
joint	0.4	8351	7703	velocity	0.4	8113	6743		0.4	3673	3724
position	0.5	8188	7615		0.5	8044	6702		0.5	3711	3641
	1.0	7580	7180		1.0	7702	6231		1.0	3420	3172

Table 23: Quantitative performance of HalfCheetah-v3 tasks with different constant coefficient settings under weight uncertainty conditions.

Type	Constant	LIF ($T=5$) Reward↑	SRM ($T=5$) Reward↑	Type	Constant	LIF ($T=5$) Reward↑	SRM ($T=5$) Reward↑	Type	Constant	LIF ($T=5$) Reward↑	SRM ($T=5$) Reward↑
	0.1	10780	11624		0.1	6798	8142		0.1	6428	5250
	0.2(original)	**10823**	**11767**		0.2(original)	**6928**	**8381**		0.2(original)	**6551**	**5386**
8-bit	0.3	10672	11584	GN	0.3	6920	8077	30%	0.3	6531	5188
Loihi	0.4	10658	11467	weight	0.4	6818	7936	Zero	0.4	6286	5102
weight	0.5	10583	11385		0.5	6674	7769	weight	0.5	6290	4975
	1.0	9757	10648		1.0	6113	7019		1.0	5680	4562

Table 24: Quantitative performance of Ant-v3 tasks with different constant coefficient settings under standard testing conditions.

Constant	LIF ($T=5$) Reward↑	SRM ($T=5$) Reward↑
0.1	5662	5803
0.2(original)	**5726**	**5879**
0.3	5648	5747
0.4	5570	5589
0.5	5394	5610
1.0	5104	5226

23

Table 25: Quantitative performance of Ant-v3 tasks with different constant coefficient settings under degraded inputs conditions.

Type	Constant	**LIF** ($T=5$) Reward↑	**SRM** ($T=5$) Reward↑	Type	Constant	**LIF** ($T=5$) Reward↑	**SRM** ($T=5$) Reward↑	Type	Constant	**LIF** ($T=5$) Reward↑	**SRM** ($T=5$) Reward↑
	0.1	3241	3368		0.1	2983	2772		0.1	1214	1478
	0.2(original)	**3339**	**3450**		0.2(original)	**3103**	**2984**		0.2(original)	**1269**	**1559**
Random	0.3	3188	3380	Random	0.3	3032	2704	GN	0.3	1148	1409
joint	0.4	3213	3217	joint	0.4	2844	2655		0.4	1003	1255
position	0.5	3062	3048	velocity	0.5	2697	2517		0.5	980	1261
	1.0	2676	2572		1.0	2230	2280		1.0	772	1083

Table 26: Quantitative performance of Ant-v3 tasks with different constant coefficient settings under weight uncertainty conditions.

Type	Constant	**LIF** ($T=5$) Reward↑	**SRM** ($T=5$) Reward↑	Type	Constant	**LIF** ($T=5$) Reward↑	**SRM** ($T=5$) Reward↑	Type	Constant	**LIF** ($T=5$) Reward↑	**SRM** ($T=5$) Reward↑
	0.1	5413	5600		0.1	2703	1596		0.1	2883	2925
	0.2(original)	**5570**	**5648**		0.2(original)	**2782**	**1658**		0.2(original)	**2931**	**3046**
8-bit	0.3	5373	5583	GN	0.3	2636	1554	30%	0.3	2945	2990
Loihi	0.4	5230	5349	weight	0.4	2488	1433	Zero	0.4	2802	2731
weight	0.5	5022	5224		0.5	2523	1382	weight	0.5	2652	2583
	1.0	4448	4783		1.0	2205	1071		1.0	2217	1992

24

Table 27: Quantitative performance of obstacle avoidance tasks under the standard static obstacle conditions with respect to random seeds.

Random Seed	**LIF** $(T = 5)$ SR↑	**SRM** $(T = 5)$ SR↑
1	**98.5%**	96%
2	**98.5%**	**96.5%%**
3	97%	95%
4	96.5%	95.5%
5	98%	96%
Mean	97.7%	95.8%
Standard Deviation	0.008	0.005
Coefficient of Variation	0.008	0.005

Table 28: Quantitative performance of obstacle avoidance tasks under dynamic obstacle conditions with respect to random seeds.

Random Seed	**LIF** $(T = 5)$ SR↑	**SRM** $(T = 5)$ SR↑
1	92%	89.5%
2	**92.5%**	**90.5%**
3	91%	90.5%
4	92%	90%
5	92.5%	89.5%
Mean	92%	90%
Standard Deviation	0.005	0.004
Coefficient of Variation	0.006	0.005

Supplementary Note 8: Impact of Random Seeds

In this section, we study the impact of the random seeds during the training process on the proposed BDETT. For the obstacle avoidance tasks, we train five models for each LIF- and SRM-based host SNN, corresponding to five different random seeds. The SRs and the corresponding error bars of the trained host SNNs are reported in Figure 7a and Tables 27, 28, 29, and 30.

For the continuous control tasks, the rewards obtained in the HalfCheetah-v3 tasks under all experimental conditions are shown in Figure 7b. The corresponding experimental results are reported in Tables 31, 32, and 33. In Tables 34, 35, and 36, we report the experimental results of the Ant-v3 tasks under all experimental settings. The results are also illustrated in Figure 7c.

Since the mean success rates and rewards obtained in the three tasks differ significantly, we calculate coefficients of variation to produce fair comparisons. We observe that the random seeds have the lowest impact on the obstacle avoidance tasks and the most substantial influence on the Ant-v3 tasks.

Table 29: Quantitative performance of obstacle avoidance tasks under degraded input conditions with respect to random seeds.

Type	Random Seed	LIF $(T = 5)$ SR↑	SRM $(T = 5)$ SR↑	Type	Random Seed	LIF $(T = 5)$ SR↑	SRM $(T = 5)$ SR↑	Type	Random Seed	LIF $(T = 5)$ SR↑	SRM $(T = 5)$ SR↑
	1	89%	79%		1	83.5%	82%		1	82.5%	81.5%
	2	**90%**	**79.5%**		2	**84.5%**	**83%**		2	**84.5%**	**82.5%**
	3	89.5%	79%		3	85%	82.5%		3	83%	81.5%
0.2	4	88%	78.5%	0.6	4	84%	81.5%	GN	4	83.5%	81%
	5	89%	78%		5	83%	82%		5	82%	82%
	Mean	89.1%	78.8%		Mean	84%	82.2%		Mean	83.1%	81.7%
	Standard Deviation	0.007	0.005		Standard Deviation	0.007	0.005		Standard Deviation	0.009	0.005
	Coefficient of Variation	0.007	0.006		Coefficient of Variation	0.008	0.006		Coefficient of Variation	0.010	0.006

25

Table 30: Quantitative performance of obstacle avoidance tasks under weight uncertainty conditions with respect to random seeds.

Type	Random Seed	LIF ($T=5$) SR↑	SRM ($T=5$) SR↑	Type	Random Seed	LIF ($T=5$) SR↑	SRM ($T=5$) SR↑	Type	Random Seed	LIF ($T=5$) SR↑	SRM ($T=5$) SR↑
8-bit Loihi weight	1	**90%**	87%	GN weight (5 rounds)	1	85.8%	61%	30% Zero weight (5 rounds)	1	76.8%	64.5%
	2	**90%**	**88.5%**		2	**87.7%**	**61.8%**		2	**77.2%**	**65.2%**
	3	88.5%	86%		3	87.1%	61.3%		3	75.9%	63.9%
	4	88.5%	88.5%		4	86.6%	60.2%		4	75.4%	64.5%
	5	89%	86.5%		5	87.5%	60.8%		5	76.9%	65.0%
	Mean	89.2%	87.3%		Mean	86.9%	61%		Mean	76.4%	64.6%
	Standard Deviation	0.007	0.010		Standard Deviation	0.007	0.005		Standard Deviation	0.007	0.005
	Coefficient of Variation	0.008	0.012		Coefficient of Variation	0.008	0.009		Coefficient of Variation	0.009	0.007

Table 31: Quantitative performance of HalfCheetah-v3 tasks under standard testing condition with respect to random seeds.

Random Seed	**LIF** ($T=5$) Reward↑	**SRM** ($T=5$) Reward↑
1	11064	11960
2	10979	11873
3	9848	10474
4	10881	11061
5	8992	11644
6	10977	10939
7	10975	11337
8	10869	11777
9	10932	10673
10	10993	11841
Mean	10651	11358
Standard Deviation	647	513
Coefficient of Variation	0.061	0.045

Table 32: Quantitative performance of the HalfCheetah-v3 tasks under degraded input conditions with respect to random seeds.

Type	Random Seed	LIF ($T=5$) Reward↑	SRM ($T=5$) Reward↑	Type	Random Seed	LIF ($T=5$) Reward↑	SRM ($T=5$) Reward↑	Type	Random Seed	LIF ($T=5$) Reward↑	SRM ($T=5$) Reward↑
Random joint position	1	8465	7883	Random joint position	1	8302	7116	GN	1	3909	3895
	2	8452	7788		2	8239	7101		2	3820	3854
	3	7617	6618		3	7575	5684		3	3292	2648
	4	8399	7001		4	8274	6208		4	3797	2979
	5	7003	7622		5	7216	6869		5	2816	3561
	6	8320	7280		6	8226	6540		6	3675	3197
	7	8339	7557		7	8288	6806		7	3790	3636
	8	8348	7832		8	8129	6805		8	3743	3582
	9	8329	6777		9	8118	6044		9	3858	2770
	10	8423	7781		10	8208	6964		10	3806	3667
	Mean	8169	7414		Mean	8058	6614		Mean	3651	3379
	Standard Deviation	454	443		Standard Deviation	345	459		Standard Deviation	322	426
	Coefficient of Variation	0.056	0.06		Coefficient of Variation	0.043	0.069		Coefficient of Variation	0.088	0.126

26

Table 33: Quantitative performance of the HalfCheetah-v3 tasks under weight uncertainty conditions with respect to random seeds.

Type	Random Seed	LIF (T=5) Reward↑	SRM (T=5) Reward↑	Type	Random Seed	LIF (T=5) Reward↑	SRM (T=5) Reward↑	Type	Random Seed	LIF (T=5) Reward↑	SRM (T=5) Reward↑
8-bit Loihi weight	1	10823	11767	GN weight	1	6928	8381	30% Zero weight	1	6551	5386
	2	10767	11749		2	6704	8307		2	6486	5308
	3	10062	10406		3	6155	7208		3	5671	3970
	4	10648	10780		4	6858	7527		4	6296	4254
	5	9368	11452		5	5857	8216		5	5217	5249
	6	10532	11097		6	6656	7537		6	6282	5007
	7	10284	11358		7	6838	8046		7	6341	5040
	8	10617	11768		8	6729	8306		8	6231	5337
	9	10788	10733		9	6740	7598		9	6537	4227
	10	10787	11496		10	6765	8282		10	6481	5081
	Mean	10468	11261		Mean	6623	7941		Mean	6209	4886
	Standard Deviation	435	460		Standard Deviation	324	407		Standard Deviation	410	501
	Coefficient of Variation	0.042	0.041		Coefficient of Variation	0.049	0.051		Coefficient of Variation	0.066	0.103

Table 34: Quantitative performance of the Ant-v3 tasks under standard testing condition with respect to random seeds.

Random Seed	LIF (T=5) Reward↑	SRM (T=5) Reward↑
1	5726	5879
2	5678	5758
3	5306	5798
4	5553	5480
5	3980	5508
6	4657	5590
7	5692	4063
8	5595	5829
9	5688	5429
10	5696	5616
Mean	5357	4933
Standard Deviation	553	500
Coefficient of Variation	0.103	0.101

Table 35: Quantitative performance of Ant-v3 tasks under degraded input conditions with respect to random seeds.

Type	Random Seed	LIF (T=5) Reward↑	SRM (T=5) Reward↑	Type	Random Seed	LIF (T=5) Reward↑	SRM (T=5) Reward↑	Type	Random Seed	LIF (T=5) Reward↑	SRM (T=5) Reward↑
Random joint position	1	3339	3450	Random joint position	1	3103	2984	GN	1	1269	1559
	2	3323	3423		2	2879	2869		2	1166	1524
	3	2973	3059		3	2651	2930		3	1030	1432
	4	3161	3049		4	2763	2731		4	1093	1357
	5	2053	3234		5	2105	2870		5	796	1440
	6	2424	3339		6	2547	2863		6	881	1396
	7	2993	2252		7	2822	2032		7	1132	830
	8	3216	3365		8	2892	2829		8	1105	1501
	9	3217	3300		9	3047	2815		9	1268	1464
	10	3218	3237		10	2860	2692		10	1020	1385
	Mean	2992	2847		Mean	2767	2492		Mean	1076	1250
	Standard Deviation	402	332		Standard Deviation	270	256		Standard Deviation	144	196
	Coefficient of Variation	0.134	0.117		Coefficient of Variation	0.098	0.103		Coefficient of Variation	0.134	0.157

27

Table 36: Quantitative performance of Ant-v3 tasks under weight uncertainty conditions with respect to random seeds.

Type	Random Seed	LIF ($T=5$) Reward↑	SRM ($T=5$) Reward↑	Type	Random Seed	LIF ($T=5$) Reward↑	SRM ($T=5$) Reward↑	Type	Random Seed	LIF ($T=5$) Reward↑	SRM ($T=5$) Reward↑
8-bit Loihi weight	1	5570	5648	GN weight	1	2782	1658	30% Zero weight	1	2931	3046
	2	5398	5641		2	2668	1503		2	2849	2859
	3	5219	5611		3	2518	1467		3	2729	2674
	4	5309	5291		4	2580	1341		4	2741	2929
	5	4395	5201		5	1816	1522		5	1840	2794
	6	4853	5394		6	2303	1466		6	2125	2730
	7	5166	3968		7	2426	959		7	2654	1895
	8	5365	5610		8	2646	1595		8	2826	2760
	9	5544	5416		9	2601	1427		9	2874	2635
	10	5254	5343		10	2422	1497		10	2802	2644
	Mean	5207	4778		Mean	2476	1294		Mean	2637	2432
	Standard Deviation	333	473		Standard Deviation	257	181		Standard Deviation	342	294
	Coefficient of Variation	0.064	0.099		Coefficient of Variation	0.104	0.140		Coefficient of Variation	0.130	0.121
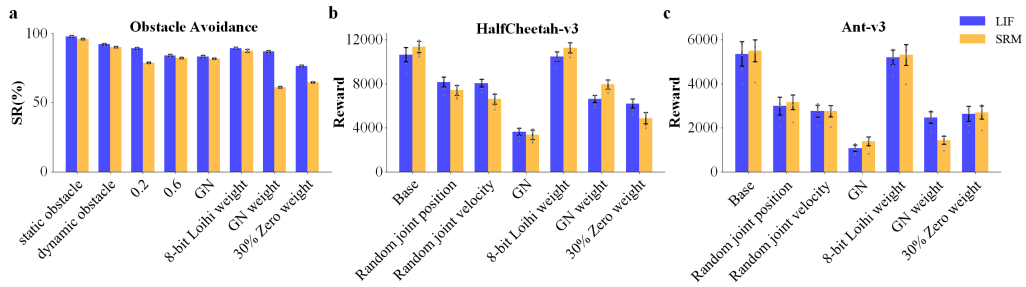
Figure 7: Quantitative performance of the LIF- and SRM-based BDETThost SNNs with respect to random seeds.

28

Supplementary Note 9: BDETT without Statistical Parameter Settings

We study the impact of the proposed layerwise statistical parameter settings, an extension of section 4.3 of our main paper. The experimental settings and the corresponding results are reported in Table 37. Without replacing the constants of the original biological model, the proposed method is is only slightly better than the ones without any training. Both LIF- and SRM-based experiments validate that the proposed statistical cues are essential to the proposed method.

Table 37: Quantitative performance of BDETT without statistical parameter settings (SPS) under the stardard testing conditions. OA means obstacle avoidance; HC-v3 indicates HalfCheetah-v3.

Approach	SPS	Trained	LIF			SRM		
			OA (SR↑)	HC-v3 (Reward↑)	Ant-v3 (Reward↑)	OA (SR↑)	HC-v3 (Reward↑)	Ant-v3 (Reward↑)
BDETT	Yes	Yes	92.5%	11064	5726	90.5%	11960	5879
BDETT	No	Yes	0%	-35	-9	0%	-28	-18
BDETT	Yes	No	0%	-124	-73	0%	-59	3

29

Supplementary Note 10: Interaction between DET and DTT

In the section "Interaction of DET and DTT" of our main paper, we illustrate the interaction between DET and DTT with two examples. Here, we provide additional experimental evidence of the interaction of DET and DTT. Without loss of generality, we conduct the experiments by using spiking actor network (SAN) as the host SNN for a robot obstacle avoidance task.

Interaction DET/DTT with low potential fluctuations.

- **Experimental setup**: We randomly chose a timestamp and recorded all postsynaptic membrane potentials and spiking thresholds of the host SNN. Then, for each layer, we randomly selected X neurons based on the binomial distribution with a probability of 0.5. The chosen neurons were added random positive noise, generated based on a normal distribution $\mathcal{N}(0.2, 0.05)$. The mean of 0.2 is around 20% of the average of the recorded membrane potentials. To reduce the impact of the randomness, we did 5-round tests and reported the average and standard deviation of the obtained DETs and DTTs. The average number of selected neurons of these 5-round tests of each layer, $\mu(X)$, is also reported.

- **Experimental thesis**: We expect DET increases as the noise increases the membrane potential. DTT should remain at a relatively constant threshold (*i.e.*, $a + 1$) as the preceding rate of depolarization caused by the noise is close to 0.

- **Experimental result**: The layerwise mean, μ, and standard deviation, σ, of the 5-round DETs and DTTs with and without added noise are reported in Table 38, aligning well with the experimental thesis. Δ is the absolute value of the difference between original and add noise.

Table 38: Interaction DET/DTT with low potential fluctuations.

	$\mu(X)$	original (μ / σ)	add noise (μ / σ)	Δ
layer 1 DET		1.4950 / 0.0051	1.5143 / 0.0066	0.0193 / 0.0015
	130.4			
layer 1 DTT		0.0570 / 0.0064	0.0571 / 0.0063	0.0001 / 0.0001
layer 2 DET		2.1548 / 0.0120	2.1745 / 0.0111	0.0197 / 0.0009
	128.4			
layer 2 DTT		0.2725 / 0.0154	0.2724 / 0.0152	0.0001 / 0.0002
layer 3 DET		3.3528 / 0.0788	3.3720 / 0.0777	0.0192 / 0.0011
	126.6			
layer 3 DTT		0.4549 / 0.0033	0.4549 / 0.0033	0.0000 / 0.0000

Interaction DET/DTT with fast membrane potential drop.

- **Experimental setup**: We adopted the same binomial distribution as in the first experiment and randomly selected X neurons of the host SNN. To mimic fast membrane potential drops from t to $t+1$, we added random negative membrane potentials with a larger magnitude than the first experiment, which was generated by sampling a normal distribution $\mathcal{N}(-2.0, 0.5)$.

- **Experimental thesis**: In this scenario, even though DET decreases with the reduced membrane potential, we expect DTT to increase faster, and BDETT to increase the overall threshold.

- **Experimental result**: The layerwise mean and STD of the 5-round X DETs, DTTs, and BDETTs with and without fast membrane potential drop are shown in Table 39. Again, the findings align with the experimental thesis.

30

Table 39: Interaction DET/DTT with fast membrane potential drop

	$\mu(X)$	**original** (μ / σ)	**fast potential drop** (μ / σ)	Δ
layer 1 DET		1.4919 / 0.0089	1.4032 / 0.0106	0.0887 / 0.0017
layer 1 DTT	128.2	0.0579 / 0.0044	1.0115 / 0.0251	0.9536 / 0.0207
layer 1 BDETT		0.7749 / 0.0039	1.2074 / 0.0124	0.4325 / 0.0085
layer 2 DET		2.1865 / 0.0292	2.0348 / 0.0514	0.1517 / 0.0222
layer 2 DTT	124.8	0.2863 / 0.0053	1.1938 / 0.0332	0.9075 / 0.0279
layer 2 BDETT		1.2364 / 0.0148	1.6143 / 0.0293	0.3779 / 0.0145
layer 3 DET		3.6456 / 0.1114	3.3802 / 0.1298	0.2654 / 0.0184
layer 3 DTT	130.4	0.4479 / 0.0141	1.3337 / 0.0307	0.8858 / 0.0166
layer 3 BDETT		2.0468 / 0.0610	2.3570 / 0.0574	0.3102 / 0.0036

31

Supplementary Note 11: Runtime Complexity analysis

The computational complexity of the proposed BDETT is bounded by the computational complexity of calculating the mean, maximum, and minimum, i.e., Eqs. 3, 4, and 6. Therefore, the upper bound of estimating BDETT complexity, $\Theta_i^l(t+1)$, is $O(n)$, where n is the number of neurons on the l-th layer. The baseline methods, DT1 and DT2, are bounded by the summation operations and offer the same upper bound, $O(n)$; see Eqs. 8 and 9 in Supplementary Note 2.

We report the layer-wise running time with PyTorch 1.2 on an i7-7700 CPU and NVIDIA GTX 1080Ti GPU. As we can see the running time of the proposed BDETT for the testing network is 1.36 ms.

Table 40: Layer-wise running time.

	Layer 1 (256 neurons)	Layer 2 (256 neurons)	Layer 3 (256 neurons)	Layer 4 (2 neurons)	Total
DET (ms)	0.18	0.19	0.19	0.18	0.74
DTT (ms)	0.11	0.11	0.11	0.10	0.43
BDETT (ms)	0.34	0.35	0.35	0.32	1.36

32

References

[1] Sumit Bam Shrestha and Garrick Orchard. Slayer: Spike layer error reassignment in time. In *Advances in Neural Information Processing Systems*, volume 31, pages 1412–1421, 2018.

[2] Wulfram Gerstner. Time structure of the activity in neural network models. *Physical Review E*, 51(1):738–758, 1995.

[3] Wulfram Gerstner and Werner M. Kistler. *Spiking Neuron Models: Single Neurons, Populations, Plasticity*. 2002.

[4] Yunzhe Hao, Xuhui Huang, Meng Dong, and Bo Xu. A biologically plausible supervised learning method for spiking neural networks using the symmetric stdp rule. *Neural Networks*, 121:387–395, 2020.

[5] Taeyoon Kim, Suman Hu, Jaewook Kim, Joon Young Kwak, Jongkil Park, Suyoun Lee, Inho Kim, Jong-Keuk Park, and YeonJoo Jeong. Spiking neural network (snn) with memristor synapses having non-linear weight update. *Frontiers in computational neuroscience*, 15:22, 2021.

[6] A.L. Hodgkin and A.F. Huxley. A quantitative description of membrane current and its application to conduction and excitation in nerve. *Journal of Physiology*, 117:500–544, 1952.

[7] Rony Azouz and Charles M. Gray. Dynamic spike threshold reveals a mechanism for synaptic coincidence detection in cortical neurons in vivo. *Proceedings of the National Academy of Sciences of the United States of America*, 97(14):8110–8115, 2000.

[8] Andrew Y. Y. Tan, Yuzhi Chen, Benjamin Scholl, Eyal Seidemann, and Nicholas J. Priebe. Sensory stimulation shifts visual cortex from synchronous to asynchronous states. *Nature*, 509(7499):226–229, 2014.

[9] David A. McCormick, Yousheng Shu, and Yuguo Yu. Hodgkin and huxley model —still standing? *Nature*, 445(7123):E1–E2, 2007.

[10] W Tackmann and HJ Lehmann. Refractory period in human sensory nerve fibres. *European neurology*, 12(5-6):277–292, 1974.

[11] Eric R. Kandel, James H. Schwartz, and Thomas M. Jessell, editors. *Principles of Neural Science*. Elsevier, New York, third edition, 1991.

[12] Wei Zhang and David J. Linden. The other side of the engram: experience-driven changes in neuronal intrinsic excitability. *Nature Reviews Neuroscience*, 4(11):885–900, 2003.

[13] Leon N Cooper and Mark F. Bear. The bcm theory of synapse modification at 30: interaction of theory with experiment. *Nature Reviews Neuroscience*, 13(11):798–810, 2012.

[14] Bertrand Fontaine, José Luis Peña, and Romain Brette. Spike-threshold adaptation predicted by membrane potential dynamics in vivo. *PLOS Computational Biology*, 10(4), 2014.

[15] Luk Chong Yeung, Harel Z Shouval, Brian S Blais, and Leon N Cooper. Synaptic homeostasis and input selectivity follow from a calcium-dependent plasticity model. *Proceedings of the National Academy of Sciences*, 101(41):14943–14948, 2004.

[16] Qian-Quan Sun. Experience-dependent intrinsic plasticity in interneurons of barrel cortex layer iv. *Journal of Neurophysiology*, 102(5):2955–2973, 2009.

[17] Karine Pozo and Yukiko Goda. Unraveling mechanisms of homeostatic synaptic plasticity. *Neuron*, 66(3):337–351, 2010.

[18] Jose Luis Pena and Masakazu Konishi. From postsynaptic potentials to spikes in the genesis of auditory spatial receptive fields. *Journal of Neuroscience*, 22(13):5652–5658, 2002.

[19] Rony Azouz and Charles M Gray. Adaptive coincidence detection and dynamic gain control in visual cortical neurons in vivo. *Neuron*, 37(3):513–523, 2003.

[20] Jonathan Platkiewicz and Romain Brette. A threshold equation for action potential initiation. *PLoS computational biology*, 6(7):e1000850, 2010.

[21] Björn Naundorf, Fred Wolf, and Maxim Volgushev. Unique features of action potential initiation in cortical neurons. *Nature*, 440(7087):1060–1063, 2006.

33

[22] Guangzhi Tang, Neelesh Kumar, and Konstantinos P Michmizos. Reinforcement co-learning of deep and spiking neural networks for energy-efficient mapless navigation with neuromorphic hardware. *arXiv preprint arXiv:2003.01157*, 2020.

[23] Adam Paszke, Sam Gross, Francisco Massa, Adam Lerer, James Bradbury, Gregory Chanan, Trevor Killeen, Zeming Lin, Natalia Gimelshein, Luca Antiga, et al. Pytorch: An imperative style, high-performance deep learning library. *arXiv preprint arXiv:1912.01703*, 2019.

[24] Jinyoung Choi, Kyungsik Park, Minsu Kim, and Sangok Seok. Deep reinforcement learning of navigation in a complex and crowded environment with a limited field of view. In *2019 International Conference on Robotics and Automation (ICRA)*, pages 5993–6000. IEEE, 2019.

[25] Scott Fujimoto, Herke Hoof, and David Meger. Addressing function approximation error in actor-critic methods. In *International Conference on Machine Learning*, pages 1587–1596. PMLR, 2018.

[26] Guangzhi Tang, Neelesh Kumar, Raymond Yoo, and Konstantinos P Michmizos. Deep reinforcement learning with population-coded spiking neural network for continuous control. *arXiv preprint arXiv:2010.09635*, 2020.

34